Tectonophysics 805 (2021) 228770

Contents lists available at ScienceDirect

Tectonophysics

journal homepage: www.elsevier.com/locate/tecto

The transition zone between the Eastern Alps and the Pannonian basin imaged by ambient noise tomography

Gyöngyvér Szanyi [a,b,*], Zoltán Gráczer [a,b], Brigitta Balázs [c], István János Kovács [a,b,d], AlpArray Working Group

[a] Kövesligethy Radó Seismological Observatory, ELKH CSFK GGI, Budapest, Hungary
[b] MTA EK Lendület Pannon LitH$_2$Oscope Research Group, Budapest, Hungary
[c] Department of Geophysics and Space Science, ELTE TTK, Budapest, Hungary
[d] Environmental Physics Laboratory, ELKH EK EKBI, Budapest, Hungary

ARTICLE INFO

Keywords:
Ambient noise tomography
Rayleigh-wave
Crustal shear velocity model
Direct inversion
AlpArray
Pannonian basin

ABSTRACT

The aim of this study was to establish a 3D shear-wave velocity model of the transition zone between the Eastern Alps and the Pannonian basin by means of ambient noise tomography. Datasets from permanent networks as well as past and recently deployed temporary networks of broadband seismic stations have been processed. Empirical Green's functions were estimated via cross-correlation of vertical component ambient seismic noise and further processed to obtain Rayleigh-wave group-velocity dispersion curves. They were directly inverted for shear velocities through a wavelet-based sparsity-constrained tomography method avoiding the intermediate step of constructing 2D group velocity maps. A horizontal resolution of 0.2° in the upper crust and 0.3°–0.5° in the lower crust was achieved. Our upper crustal shear velocity model revealed low velocities in the sedimentary depocenters and high velocities below the surrounding mountains. However, at greater depths (24–29 km), high shear velocities beneath the basins suggest crustal thinning accompanied by mantle updoming. An extremely deep low velocity anomaly was mapped beneath the Vienna basin, which we argue is caused by either sediment transfer to the lower crust; ductile deformation suggested by seismic anisotropy; or the presence of fluids.

1. Introduction

The Pannonian basin is a major extensional back-arc basin in the convergence zone between the Adriatic microplate and the stable European Platform, surrounded by the Alps, the Carpathians and the Dinarides (Fig. 1). The pre-Tertiary basement consists of two main structural domains: 1) the ALCAPA (Alps-Carpathians-Pannonian) micro-terrain in the northwest, 2) the Tisza-Dacia micro-terrain in the southeast separated by the Mid-Hungarian Zone (MHZ) which lies between the Balaton Line (in the north) and the Mid-Hungarian Line (in the south) and forms a major shear zone (Haas et al., 2014). In the study area the ALCAPA unit is bound to the Bohemian Massif on the W and NW with a relatively narrow zone of the External Western Carpathians (EWC) and the Molasse Basin in between consisting mainly of younger sediments.

These main structural units of the Pannonian basin have different origin and history. The ALCAPA unit belongs to the African Plate. It is still under dispute, whether its eastward extrusion and later counter-clockwise rotation starting in the Late Oligocene and Early Miocene occurred only on crustal levels or affected the entire lithosphere. Models proposing gravitational collapse of the Alps imply that only the upper crust took part in the lateral escape (Ratschbacher et al., 1991; Ranalli, 1995). Alternatively, some studies (Kovács et al., 2012; van Gelder et al., 2017) argued that the extrusion affected the entire lithosphere. According to paleomagnetic measurements the ALCAPA unit rotated counter-clockwise during the Neogene (Márton et al., 2000; Márton and Fodor, 2003). However, the Tisza-Dacia micro-terrain has broken off from the Variscan Orogenic Zone of the Eurasian Plate (Haas et al., 2014) and experienced clockwise rotation. The two oppositely rotating micro-terrains is joined by the Mid-Hungarian Zone, which is a few tens of kilometres wide and approximately 450 km long, SW-NE oriented relatively narrow region, built up of the remnants of oceanic realms (Penninic, Magura, Vardar) (Csontos and Vörös, 2004; Schmid et al., 2008). The structure and evolution of this very important unit is still disputed.

The Pannonian basin includes several smaller sub-basins separated

* Corresponding author at: Kövesligethy Radó Seismological Observatory, ELKH CSFK GGI, Budapest, Hungary.
E-mail address: szanyi@seismology.hu (G. Szanyi).

https://doi.org/10.1016/j.tecto.2021.228770
Received 26 May 2020; Received in revised form 31 January 2021; Accepted 3 February 2021
Available online 12 February 2021

by elevated basement topography and filled with several kilometres thick young, unconsolidated sediments.

The NE-SW oriented Vienna basin is situated roughly between the SE edge of the Bohemian Massif and the Little Carpathians. Deep geophysical surveys revealed that the (upper) crust of the Bohemian Massif intrudes further to the SE underneath the basement of the Vienna basin and it extends as far as the Little Carpathians (Šamajová et al., 2018, 2019). This basin is regarded as one of the best examples of rhombohedral shaped strike-slip basins formed in orogenic belts (Royden, 1985). Its fault systems in the uppermost crust, and the present-day active faults have been thoroughly studied with various methods (e.g. Fodor, 1995; Decker et al., 2005; Hölzel et al., 2010; Hinsch and Decker, 2011; Baroň et al., 2019). The basin is separated from the SE situated, younger and roughly parallel Danube Basin by the Little Carpathians (Lankreijer et al., 1995; Tari, 1996; Sztanó et al., 2016). The formation of these two basins is driven by the eastward extrusion and counter-clockwise rotation of the ALCAPA plate (e.g. Nemcok et al., 1989; Fodor, 1995; Lankreijer et al., 1995; Hölzel et al., 2010; Lee and Wagreich, 2017; Kováč et al., 2018).

In the Eastern Alps, adjacent to the Pannonian basin, Penninic and Austroalpine nappes are at the surface. These nappes continue in the basement of the Danube basin and reappear as outcrops in the Transdanubian Range (Tari and Horváth, 2010). The Zala basin is located at the southwestern end of the Transdanubian Range and was formed during Miocene times with significant strike slip motions in the vicinity of the Mid-Hungarian Zone and reactivation of older thrust planes. Several NW oriented synclines and anticlines were generated during the tectonic inversion stage with thick sediment deposition (>2 km) since the Late Miocene (Fodor et al., 1999; Horváth et al., 2006; Bada et al., 2007).

Located south to the Mid-Hungarian Zone, the Drava and the Sava Basins are Early – Middle Miocene extensional basins whose present strike is WNW-ESE and they are filled with several km thick sediments (Lučić et al., 2001; Sebe et al., 2020). In SW Hungary, the Mecsek is a moderately elevated inselberg comprising Variscan Crystalline basement and Mesozoic sedimentary rocks (Csontos et al., 2002).

Starting in the Late Miocene (~11 Ma) alkaline basaltic volcanic activity took place in the Carpathian-Pannonian region (Kovács et al., 2020), which started in the Styrian basin-Burgenland area and was at its peak at 2–6 Ma in most places (Pécskay et al., 2006). It created several volcanic fields: at the SW termination of the Transdanubian Range (the Bakony Balaton Highland Volcanic Field); at the SW margin of the Danube basin (Little Hungarian Plain Volcanic Field) and the Central Slovakian Volcanic Area (Nógrád-Gömör Volcanic Field). The youngest members of these alkaline basaltic volcanoes are located at the Southern Carpathians (Perşani Mts. Volcanic Field) and the Central Slovakian Volcanic Area (Kovács et al., 2020).

The upper crustal structure, especially the sedimentary formations and the pre-Tertiary basement depth (Fig. 2a) of the Pannonian basin are thoroughly studied by a large number of shallow seismic reflection profiles and borehole data for petroleum exploration (e.g. Horváth, 1995; Tari and Horváth, 2006).

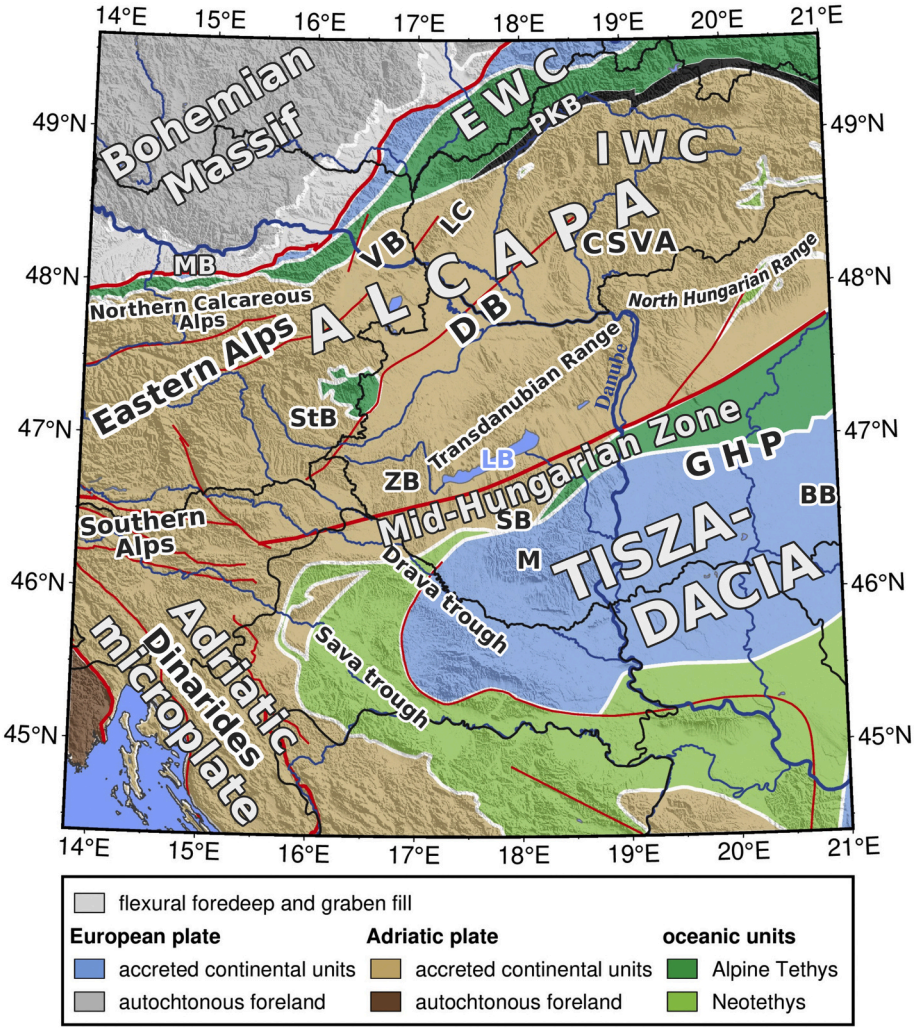

Fig. 1. Tectonic map of the study region modified after Schmid et al. (2008) and geographical features. BB – Békés basin, CSVA – Central Slovakian Volcanic Area, DB – Danube basin, EWC – External Western Carpathians, GHP – Great Hungarian Plain, IWC – Inner Western Carpathians, LB – Lake Balaton, LC – Little Carpathians, M – Mecsek, MB – Molasse basin, PKB – Pieniny Klippen Belt, StB – Styrian basin, SB – Somogy basin, VB – Vienna basin, ZB – Zala basin. The territory of Hungary west to the Danube is referred to as Transdanubia.

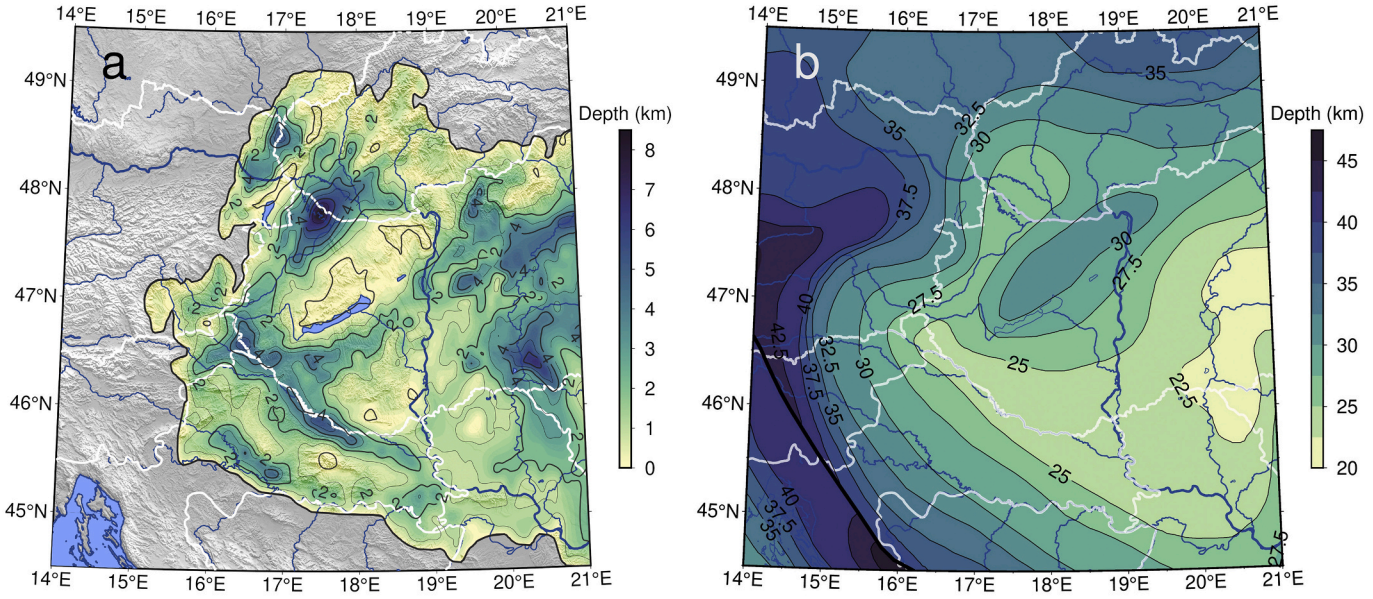

Fig. 2. a) Pre-Tertiary basement depth at the study area after Kilényi and Šefara (1989). The deepest part of the basement is located in the territory of the Danube basin, where the sedimentary thickness reaches approximately 8 km. b) Moho depth in the study area after Horváth et al. (2015). Thickening of the crust can be observed outwards from the basin area.

Most of our knowledge of the lower crustal structure comes from deep seismic reflection and refraction studies (e.g. Brückl et al., 2003; Guterch et al., 2003, 2007; Janik et al., 2011), seismic tomography (Bus, 2004; Dando et al., 2011; Ren et al., 2013; Szanyi, 2016; Timkó et al., 2019), receiver function studies (Hetényi and Bus, 2007; Hetényi et al., 2015; Kalmár et al., 2019) and magnetotelluric measurements (e.g. Ádám and Bielik, 1998; Ádám et al., 2017). The crust is significantly thinned as a result of the Miocene extension (e.g. Horváth et al., 2006; Molinari and Morelli, 2011; Kovács et al., 2012). Horváth (1993) defined the area of the Pannonian basin as the 30 km isobath of the Moho, which encircles the basin system (Fig. 2b). According to Horváth et al. (2015) the average crustal thickness is around 25 km. However, beneath the Békés basin in the Great Hungarian Plain it is even less than 22 km (Horváth et al., 2006), while it exceeds 30 km beneath the Transdanubian Range.

According to the seismic refraction profiles of the CELEBRATION2000 project (e.g. Hrubcová et al., 2010; Janik et al., 2011) and the receiver function analysis of Hetényi et al. (2015) the ALCAPA and Tisza terrains cannot be distinguished based on crustal thickness. However, beneath the MHZ Hetényi et al. (2015) could not identify clear Moho conversions, therefore the Moho depth was not determined there. The magnetic and Bouguer anomaly map of the central Pannonian basin shows linear features aligned with the MHZ (Kiss, 2016), the magnetic map reflects the Neogene volcanism (Szabó et al., 1992; Harangi et al., 2007; Kovács and Szabó, 2008) in the region.

Although the presence of the MHZ is known from seismic reflection profiles (e.g. Horváth et al., 2015), it is not clear, whether it can be traced down to the Moho. To study deep structures, seismic tomography is one of the most advanced tools. Such studies of the Pannonian basin have a spatial resolution in the order of 60–100 km (e.g. Bus, 2004; Dando et al., 2011; Ren et al., 2013; Szanyi et al., 2013; Szanyi, 2016; Timkó et al., 2019) and do not provide detailed information of the shallow and mid-crustal structures.

Ambient noise-based tomography (ANT) is a form of surface wave tomography as it also uses dispersion measurements, however the dispersion curves are obtained through cross-correlation of simultaneous noise recordings at station pairs instead of earthquake generated surface waves (e.g. Shapiro and Campillo, 2004; Bensen et al., 2007). The period range of dispersion measurements are determined by the interstation distances, the greater the distance, the longer periods of dispersion curves can be used. As surface waves are primarily sensitive to shear wave velocities, ANT is applied to resolve S-wave velocity distribution. Shear wave velocities are sensitive mainly to rock density, composition, temperature and the presence of fluids, therefore surface wave tomography is an excellent tool for exploring both crustal and upper mantle structures. A dense seismic array is ideal to perform ANT both in regional and continental scale (e.g. Yang et al., 2007; Bensen et al., 2009; Ritzwoller et al., 2011; Molinari et al., 2015; Fang et al., 2015; Legendre et al., 2017; Yudistira et al., 2017; González-Vidal et al., 2018; Schippkus et al., 2018; Bem et al., 2020).

In order to better understand the structure, evolution and geodynamics of the Alps-Apennines-Carpathians-Dinarides orogenic system the AlpArray Seismic Network was created through a transnational research initiative with more than 600 seismological stations involved and an average of 50 km interstation distance was reached in the territory and surroundings of the Alps (e.g. Hetényi et al., 2018; Gráczer et al., 2018). Thus, the data provided by the AlpArray project allow an unprecedented high-resolution seismological imaging of the region. Our study area, the transition zone between the Eastern Alps and the Pannonian basin, lies at the eastern boundary of this network.

The aim of our research was to delineate large scale sedimentary and tectonic features in the crust through the determination of 3D shear wave velocity structure, in order to contribute to a deeper understanding of the tectonics and geodynamics of the transition zone.

In this study we build a high-resolution 3D crustal shear wave velocity structure model for the transition zone between the Eastern Alps and the Pannonian basin by performing ANT with a direct inversion method proposed by Fang et al. (2015). Then, we use checkerboard tests to estimate resolution capability and reliability of the results. Finally, velocity anomalies are mapped, discussed, interpreted and compared with previous studies.

2. Data and method

2.1. Data

In order to process all available broadband data from the study area, we have collected recordings from several temporary measuring

campaigns that took place in the Pannonian basin in the last decades.

In the frame of the Carpathian Basin Project (CBP, e.g. Hetényi et al., 2009; Dando et al., 2011) a network consisting of Guralp CMG-6TD 30s sensors have been installed across Austria, Hungary and Serbia along 3 parallel lines where stations were spaced at ~30 km intervals, with approximately 40 km between each line (Dando et al., 2011). They collected data between May 2006 and August 2007. In this study 47 of these stations have been used.

As a continuation of the CBP, the network of the South Carpathian Project (SCP) operated from June 2009 to June 2011. Its stations have been deployed east of the former CBP stations, along four roughly parallel lines extending in Hungary, Romania and Serbia. The network consisted of Guralp equipment, either CMG-40T, CMG-3T or CMG-6TD sensors were used (Ren et al., 2012). We have utilised data from 14 of these stations.

The AlpArray project is an international seismological endeavour with the Alpine orogen in its focus. It has officially started at 1 January 2016 and ended at March 31, 2019. The average interstation distance for the AlpArray network (doi:10.12686/alparray/z3_2015doi:10.12686/alparray/z3_2015) was approximately 50 km. In Hungary, the temporary AlpArray stations were equipped with Guralp CMG-3T 120 s seismometers, except three stations that used Trillium Compact 120 s sensors (Gráczer et al., 2018). Further information on the AlpArray network can be found in Hetényi et al. (2018). In this study, we have processed recordings of 69 AlpArray stations for the time interval 2016–2018.

The data of each temporary network was complemented with the noise recordings of the broadband permanent stations available at that time. As a result, we have acquired data from 65 permanent stations from the following networks: Croatian Seismograph Network (doi: https://doi.org/10.7914/SN/CR), University of Zagreb, Croatia; Czech Regional Seismic Network (doi: https://doi.org/10.7914/SN/CZ), Institute of Geophysics, Academy of Sciences of the Czech Republic, Czech Republic; GEOFON Seismic Network (doi: 10.14470/TR560404), Deutsches GeoForschungsZentrum, Germany; German Regional Seismic Network (doi: 10.25928/MBX6-HR74), Federal Institute for Geosciences and Natural Resources, Germany; Hungarian National Seismological Network (doi:10.14470/UH028726), CSFK GGI KRSZO, Hungary; Mediterranean Very Broadband Seismographic Network (doi: 10.13127/SD/ FBBBTDTD6Q), MedNet Project Partner Institutions; Austrian Seismic Network (doi: https://doi.org/10.7914/SN/OE), Central Institute for Meteorology and Geodynamics, Austria; Polish Seismological Network, Polish Academy of Sciences, Poland; Serbian Seismological Network, Seismological Survey of Serbia, Serbia; National Network of Seismic Stations of Slovakia (doi: 10.14470/FX099882), Earth Science Institute of the Slovak Academy of Sciences, Slovakia; Seismic Network of the Republic of Slovenia (doi: https://doi.org/10.7914/SN/SL), Slovenian Environment Agency, Slovenia.

We have obtained the data of CBP and SCP projects from the IRIS (Incorporated Research Institutions for Seismology) data management system. We collect the recordings of the Hungarian permanent and AlpArray stations locally at the CSFK GGI Kövesligethy Radó Seismological Observatory. Data for the rest of the temporary and permanent broadband stations in the study area were downloaded through the European Integrated Data Archive (EIDA). The location of the stations is shown in Fig. 3.

2.2. Obtaining dispersion curves

We have used the vertical component seismograms for Rayleigh wave group velocity determination. Cross-correlation and frequency-time analysis were carried out using the software package "Seismic noise tomography" by Goutorbe et al. (2015). We followed the pre-processing procedure described by Bensen et al. (2007) and Goutorbe et al. (2015). The main steps were: (1) removing instrument response, mean and trend, (2) bandpass filtering between 2 and 60 s period and

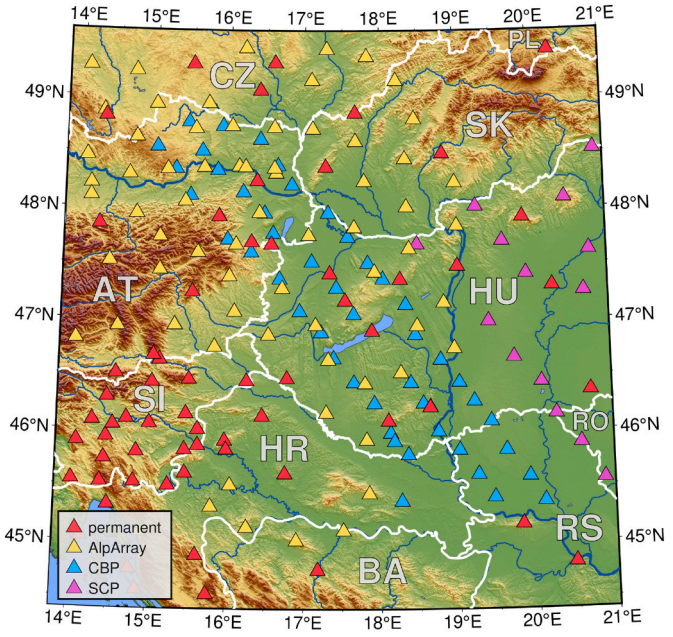

Fig. 3. Topographic map of the investigated area showing station locations: red triangles – permanent stations; yellow triangles – the temporary AlpArray stations operating since 2016 (Gráczer et al., 2018; Hetényi et al., 2018); blue triangles – the temporary stations of the Carpathian Basin Project 2005–2007 (Dando et al., 2011). Country codes are indicated in gray. (For interpretation of the references to colour in this figure legend, the reader is referred to the web version of this article.)

resampling to 1 Hz, (3) time-domain normalization using running-absolute-mean normalization and (4) spectral whitening.

The CBP, SCP and AlpArray projects collected data in different time frames, resulting in three datasets without any overlapping time period. Their recordings were used to extract the symmetrised cross-correlation functions (CCFs). Interstation distance varied between 10 and 694 km. The obtained cross-correlograms have been merged into a single collection for further processing. Fig. 4 shows the normalized CCFs as a function of interstation distance.

Rayleigh wave group velocity dispersion curves (Fig. 5a) were measured by automatic frequency-time analysis of CCFs (Levshin and Ritzwoller, 2001; Goutorbe et al., 2015). The cut-off period was set to two wavelengths. Quality control of the dispersion curves was carried out in several steps. The group velocity values of the automatically generated dispersion curves were preserved or rejected based on the signal-to-noise ratio (SNR) at each period. In order to calculate the SNR signal windows were selected with propagation velocities 1.8 and 4.2 km/s, while the noise window was always set to be the last 50 s of the time window. At a given period, the group velocity value was retained if the standard deviation calculated based on three-month stacks of data was below 0.1 km/s and the SNR was larger than 7 or, when the standard deviation was not definable, the SNR was larger than 15.

After the SNR based automatic selection, some geophysically unrealistic dispersion curves remained, which were manually removed in order to improve the input data quality for tomography.

The number of group velocity values as a function of period (Fig. 5b) varies between 773 and 5924. Between 6 s and 22 s the number of the observed group velocity values exceeds 4000, the maximum is located around 11 s period.

2.3. Three-dimensional inversion

Usually, the S-wave velocity structure is derived from dispersion curves through several consecutive steps. First, a 2D surface wave

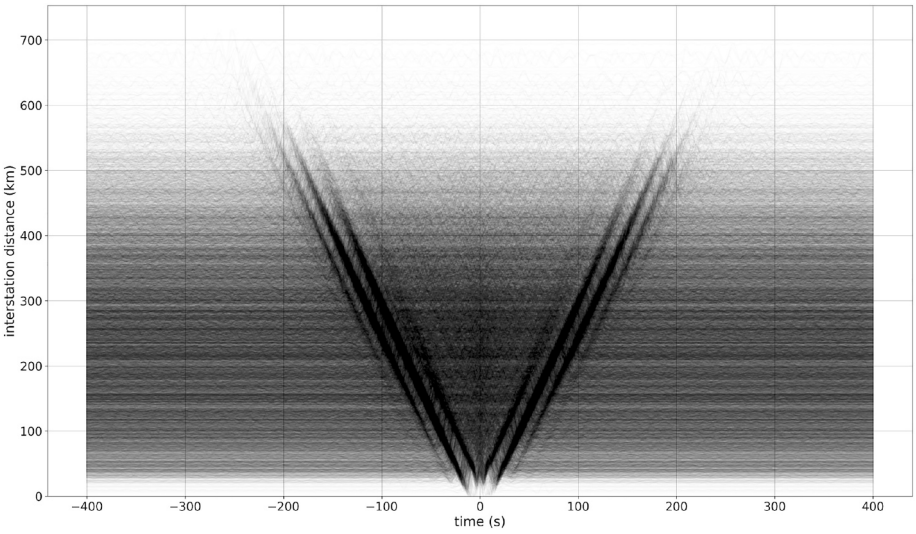

Fig. 4. All of the normalized CCFs stacked according interstation distance, filtered between 10 s and 40 s.

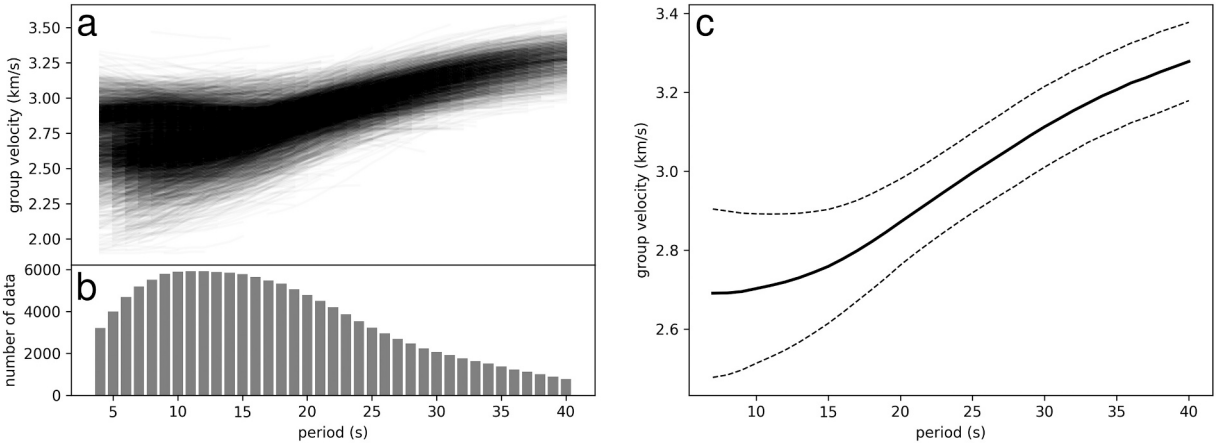

Fig. 5. a) Rayleigh-wave group velocity dispersion curves. b) The number of group velocity measurements at each period used for the tomographic computations. Selection criteria for dispersion curves is described in Section 2.2. c) Average group velocity curve, which was inverted in order to get an initial 1D velocity profile for 3D inversion. The dashed lines indicate standard deviations.

tomography is carried out; the resolution of the obtained group and/or phase velocity maps can be estimated for each period. Then a pointwise inversion is performed using the 2D maps to obtain 1D shear wave velocity profile at each point. Finally, a pseudo-3D velocity structure is built up from the ensemble of the 1D models. As a result, the resolution of the acquired 3D velocity structure is usually not estimated, only the uncertainty of the 1D inversion is specified.

To create a true 3D shear wave velocity model and to overcome the issue of the unknown resolution, we have directly inverted the dispersion curves for 3D S-wave velocity structure using the *DSurfTomo* software by Hongjian Fang that realizes a wavelet-based sparsity-constrained tomography method described in Fang and Zhang (2014) and Fang et al. (2015). This method avoids the intermediate step of constructing 2D group velocity maps and a direct inversion is achieved allowing resolution analysis of the obtained S velocity model. Beyond its most notable feature there are further advantages to this method.

First, the multiscale property of wavelet representation allows to solve the model at different scales, from coarser to finer ones, achieving to become data- and model adaptive. This is acquired through the usage of a lifting scheme when performing the wavelet transform, the original model is decomposed into approximation coefficients representing smooth components and detail coefficients describing fine scale features. In areas of poor data constraint only the approximation coefficients can be resolved and the detail coefficients are damped to zero, thus only large-scale alterations are mapped. However, in areas with good data coverage both approximation and detail coefficients are determined, resulting in higher resolution.

The ray tracing technique of *DSurfTomo* software has to be also mentioned, as it accounts for curved ray paths by using the fast marching method described in Rawlinson and Sambridge (2004). This is especially important in our work, because strong lateral variations are present in the study area. During the inversion process, the velocity kernels are updated at each iteration step.

This direct inversion procedure and *DSurfTomo* was used in several studies (e.g. Singer et al., 2017; Hu and Yao, 2018; Zhang et al., 2018; Luo et al., 2019).

In order to create an initial 1D velocity model for tomographic computations, we have constructed an average dispersion curve from the selected ones (see Section 2.2, Fig. 5c) and inverted it using the *surf96* program by Herrmann and Ammon (2002) to get a shear wave velocity profile. Depth sensitivity kernels of Rayleigh wave group velocity were computed based on this 1D velocity profile. The sensitivity analysis (Fig. 6) shows that Rayleigh waves at 4 s period are especially sensitive to the shear wave velocities in the uppermost crust, namely the

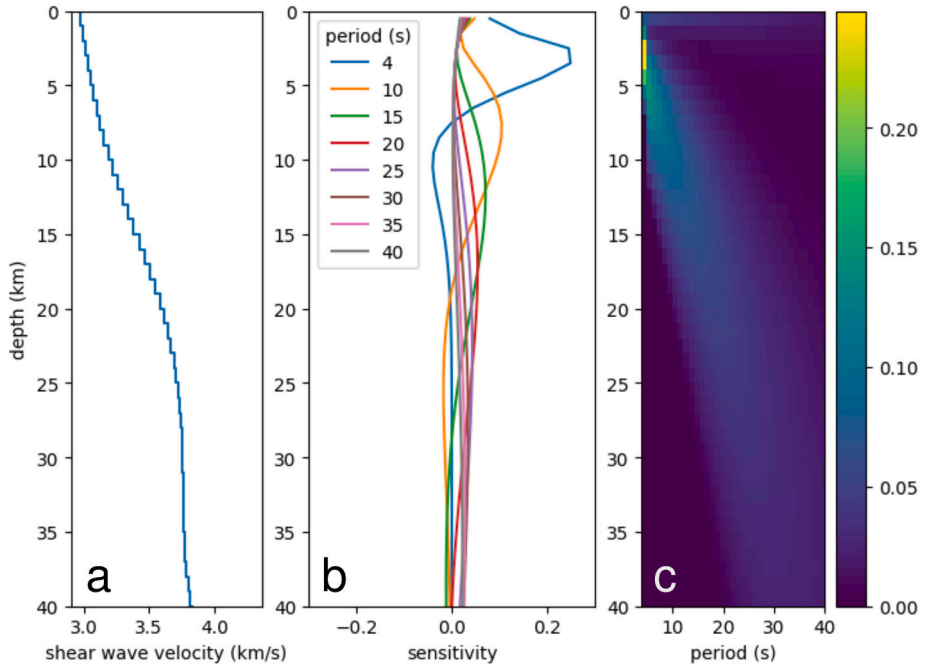

Fig. 6. Sensitivity analysis. a) The initial 1D shear wave velocity profile used for direct inversion of surface waves. b) Depth sensitivity kernels of the fundamental mode Rayleigh waves at selected periods derived from the 1D velocity model. c) Depth sensitivity kernels for all periods.

upper 6 km with a peak at ~3–4 km. Rayleigh wave group velocities at a period of 10 s are greatly influenced by the upper crustal S velocities between 4 km and 12 km. Larger periods are sensitive to greater depths, waves of a period of 20 s sample almost the entire crust (except for the upper 5 km) in the study region. Periods around 30–40 s reflect the S-wave velocity structure in the lower crust and uppermost mantle.

To perform the tomographic calculations a 3D grid should be initialized. The grid spacing was set to 0.1° horizontally. Vertically, 3 km grid spacing was used in the upper 9 km, then 5 km was applied to a depth of 39 km. The distribution of traveltime residuals of the initial and final model are shown in Fig. 7.

3. Resolution tests

To assess the spatial resolution of the inverted 3D shear wave velocity model, we conducted checkerboard tests with increasing anomaly sizes from 0.2° to 0.8° in 0.1° steps. The perturbation of the velocity value was ±10% relative to the reference 1D model.

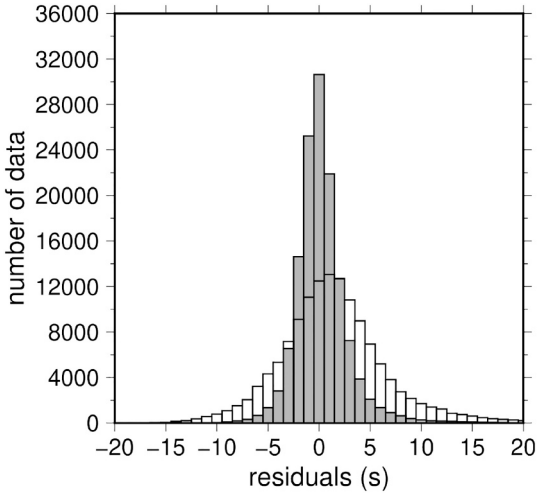

Fig. 7. Traveltime residuals before (white) and after (gray) inversion.

The model grid, ray-path coverage (Fig. 8), weighting factor and damping parameter for the checkerboard tests was the same as those used for inverting the observed data. Recovered structures at 0, 3, 19, 24, 29 and 34 km depths are shown in Fig. 9. The well resolved area (which is surrounded by a white contour line in Figs. 9 and 10.) was defined based on the results of the tests with various anomaly sizes and it was chosen to be representative at every depth. The size of the smallest anomaly that can be mapped varies with depth. At the surface 0.2° anomalies can be recovered, however they appear diagonally somewhat smeared. Between 3 km and 19 km the restored pattern is very similar for all depth sections and even anomalies with size of 0.2° can be resolved. Deeper than this, the minimal recoverable anomaly sizes grow with depth, at 24 km depth it is 0.3°, while at 29 km depth it is 0.4°. Although the checkerboard pattern of the 0.5° anomalies can be still recognized at 34 km depth, they display significant diagonal smearing.

Supplementing the previous measurements with the AlpArray data allowed us to significantly increase the 0.6° resolution achieved by Ren et al. (2013) for the study area. The analysis has shown that anomalies larger than 0.2° can be mapped with our dataset in the upper and middle crust, however the amplitude of the velocity anomaly is often slightly underestimated. In the lower crust, anomalies of 0.3°-0.4° in diameter can be well resolved, while in the uppermost mantle the minimum recoverable anomaly size is 0.4°-0.5°.

4. Results and discussion

4.1. General overview

We have computed crustal shear wave velocity structure in the Eastern Alps – Pannonian basin transition zone using vertical component cross-correlation functions of ambient noise recordings and a direct inversion method of dispersion curves (Fang et al., 2015). Horizontal velocity slices at 0, 6, 9, 19, 24, 29 km depths are shown in Fig. 10, the vertical cross-sections are shown in Fig. 11.

The velocity distribution at shallow depths is consistent with upper crustal geological features. The lowest shear velocities can be observed in the local sedimentary basins (Fig. 10). The most prominent ones are

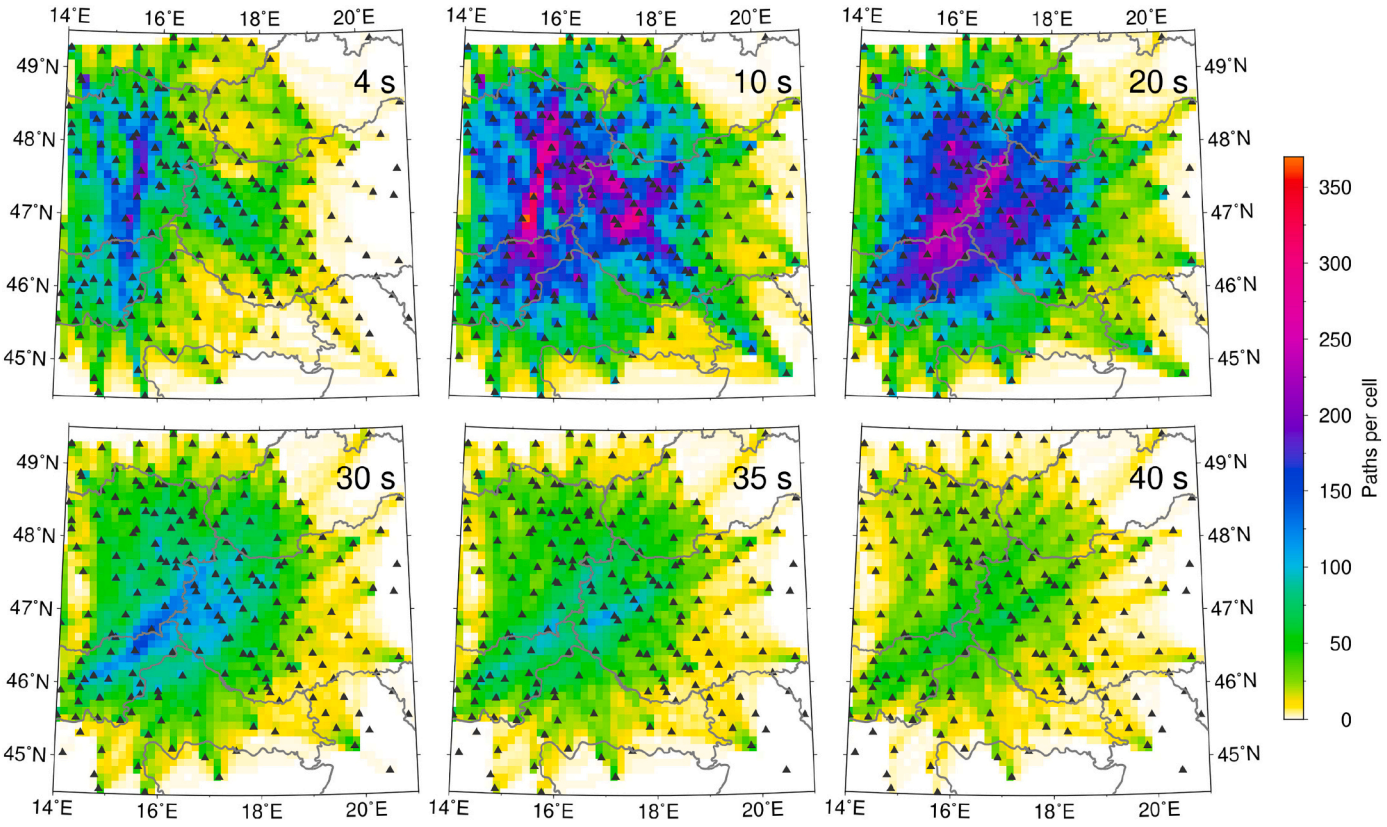

Fig. 8. Path coverage at different periods indicated in the upper right corner. The cell sizes were 0.1°x0.1°, equal to the horizontal grid spacing of the tomographic calculations. Black triangles show station locations.

the Danube basin and the Vienna basin, but the Zala basin, the Drava and Sava trough, and the Somogy basin appears as low velocity anomalies as well (for geographic units of the study area see Fig. 1).

Near-surface high velocities coincide with the locations of exposed basements. Within western Hungary the Transdanubian Range and the Mecsek appear as slightly higher velocity anomalies in the upper crust. The large mountain ranges, such as the Eastern Alps, the Western Carpathians and the Dinarides can be characterized with relatively high, 3.0–3.4 km/s shear wave velocities at shallow depths as well. The Bohemian Massif presents itself with high shear velocities in the entire crust (Fig. 11, profile AA'), it can be characterized with velocities over 3.6 km/s at a depth of 8 km and below.

At mid-crustal depths, the most pronounced feature is observed beneath the Vienna basin, which appears as a very low-velocity anomaly and is visible from the surface to the lower crust, even to a depth of 25 km or more (Fig. 11, profiles AA' and EE'). Considering the entire study region, the anomaly pattern at 9 km depth is very similar to the pattern at 6 km, although shear velocities increase in general.

At 19 km depth, the Vienna basin still presents a low velocity anomaly, however, beneath the Danube basin and the other smaller basins higher velocities can be observed. The slightly negative anomaly of 3.3 km/s in western Hungary striking NE-SW corresponds to the Transdanubian Range, and most of the mountain ranges, such as the Eastern Alps and the Dinarides also display low velocity anomalies. However, beneath the Western Carpathians higher velocities can be observed at this depth.

In the lower crust, the highest observable velocities correspond mainly to the sedimentary basin areas, while the low velocities can be observed beneath the Eastern Alps. It should be noted, that at 24 km depth high velocities occur beneath the Bohemian Massif, but the Vienna basin is still mapped as a low velocity anomaly compared to the other parts of the study area. Beneath the Transdanubian Range at 24 km depth a weak low velocity anomaly is present, however, at 29 km depth velocities beneath western Hungary are quite similar. The highest shear wave velocities at 29 km depth can be observed beneath the Danube basin and the Drava basin. The Dinarides are mapped as low anomalies as well, but high velocities can be observed beneath the Western Carpathians.

The Miocene extension of the Pannonian basin caused significant crustal and lithospheric thinning; therefore, the average crustal thickness in the Pannonian basin is less, than the continental average (e.g. Molinari and Morelli, 2011; Artemieva and Thybo, 2013). This is reflected in our tomographic images, where high velocities were mapped at 24 km depth beneath the most of the basin area constraining the Moho around this depth.

In the transition zone between the Eastern Alps and the Pannonian basin, the lithospheric thickness is rapidly changing (Horváth et al., 2006). According to the numerical simulations of Liu and Shen (1998), a steep change in lithospheric thickness may induce a lateral pressure gradient which tends to cause a lateral ductile flow within both the mantle lithosphere and even the lower crust, enhancing the thinning effect beneath the basin area and increasing crustal and lithospheric thickness around it. This phenomenon was observed between the Basin and Range province and Sierra Nevada (Liu and Shen, 1998) or beneath the Ordos Block and the Yinshan Mountains (Tian et al., 2011) and is likely to occur in the studied transition zone.

4.2. *A priori geophysical information*

In order to evaluate our shear velocity model, it is worth reviewing the existing knowledge about crustal shear velocities. Due to easier measurement of P than S velocities, the former ones are globally better mapped; however, shear wave velocities can be derived from them provided that the Poisson's ratio is known. Christensen and Mooney

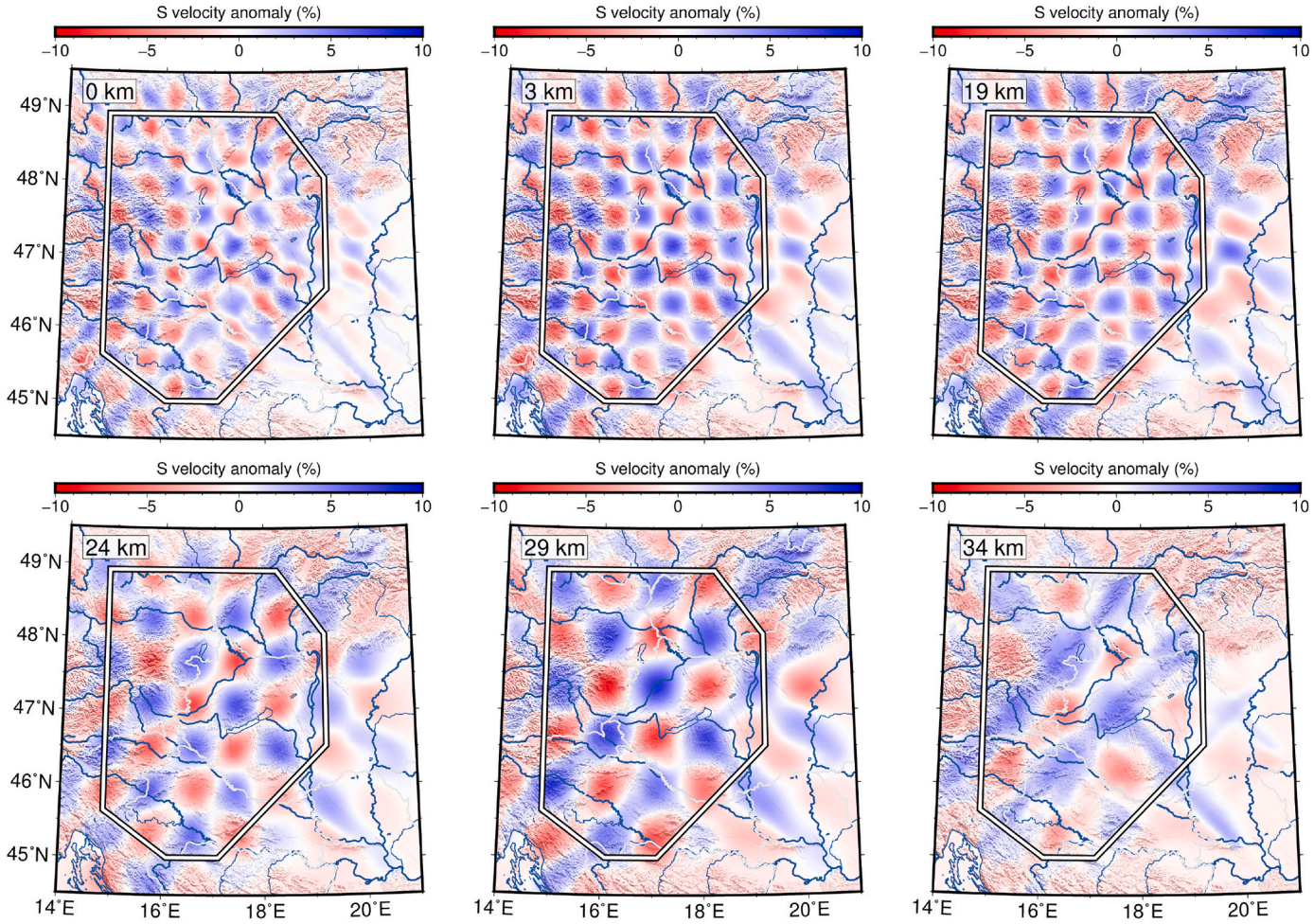

Fig. 9. Recovered checkerboard patterns at different depths (depth is shown in the upper left corner). At 3–19 km the pattern is very similar at every depth. The well recovered area is marked by white line.

(1995) and Mooney et al. (1998) have collected seismic refraction and wide-angle reflection data in order to create a global crustal structure model and developed the corresponding shear velocity model. This model was further refined by Bassin et al. (2000) and Laske et al. (2013), including velocities from surface wave and receiver function studies. The CRUST1.0 model (Laske et al., 2013) for the study area shows that shear velocities greatly vary in the sedimentary cover, they can be as low as 1.07 km/s or as high as 2.59 km/s. However, in the crystalline crust, the shear velocity is quite steady, being around 3.6 km/s, with the exception of the lower crust, where it can reach ~4 km/s. Shear velocities in the uppermost mantle vary from 4.37 to 4.5 km/s.

Seismic velocities have a strong correlation with density (Brocher, 2005; Tondi et al., 2019), higher shear velocities correspond to greater densities. The generally positive Bouguer anomaly of the study region (Bonvalot et al., 2012, Fig. 12) indicates that the upper mantle is in an elevated position (crustal thinning, e.g. Molinari and Morelli, 2011; Horváth et al., 2015; Bielik et al., 2018). The Bouguer anomaly map shows negative anomalies only at the Eastern Alps, indicating crustal thickening beneath the mountain range. This is in good agreement with our shear wave velocity model, where relatively low velocities can be observed in the deepest examined depth beneath the Eastern Alps.

Shear velocities in the crust are influenced mostly by rock composition, but temperature is also an important factor. The surface heat flow map of the Pannonian basin and the surrounding areas (Lenkey et al., 2002, 2017) shows relatively high values within the basin area, especially in the Danube basin, southwestern Hungary and the Great Hungarian Plain, where it is above 100 mW/m^2. In the meantime, the Vienna basin can be characterized by lower surface heat flow than these areas. The Bohemian Massif shows values close to the mean value of continental crust, while surface heat flow in the mountains made of limestones, e.g. the Transdanubian Range and the Northern Calcareous Alps is low due to karstic water flow (Lenkey et al., 2002, 2017).

4.3. Danube basin

The Danube basin is the deepest sedimentary basin of the study area, with 2–8 km thick sediments (Fig. 2a; Kilényi and Šefara, 1989). It is bordered by the Easter Alps and the Little Carpathians from the west, by the Western Carpathians from the north, and by the Transdanubian Range from SE. Although the Pannonian basin presents itself as a positive anomaly on the Bouguer anomaly map indicating general crustal thinning, the Danube basin appears as a relatively low Bouguer anomaly territory, probably due to the low-density, unconsolidated sedimentary filling. Low shear velocities often correspond to low densities in the crust, which is reflected in the shown depth sections (Fig. 10) and cross sections (Fig. 11). Velocities as low as 2.5 km/s were mapped near the surface, which is in good agreement both with the velocities of the CRUST1.0 model (Laske et al., 2013) and the tomographic results of Ren et al. (2013). The bottom of the Danube basin inclines upward mildly towards the Transdanubian Range and slightly steeper towards the Eastern Alps (Fig. 11., profile DD'), creating an asymmetric basement. The low shear velocities can be tracked down to 8–10 km in the cross-sections (e.g. Fig. 11, profile DD'). In the lower crust shear velocities gradually increase with depth from ~3.2 km/s at ~10–12 km to 3.6 km/

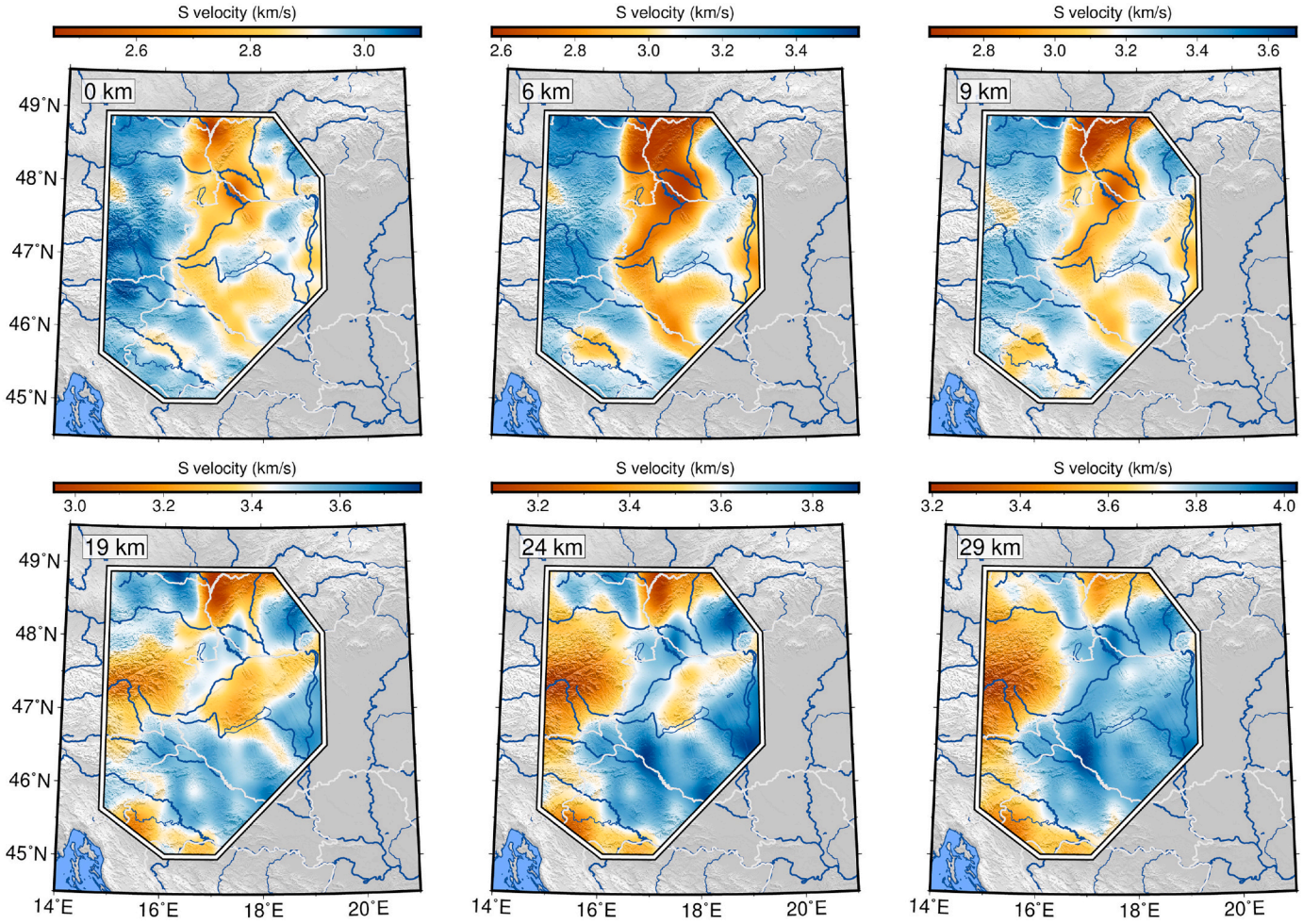

Fig. 10. Depth sections of the obtained 3D shear wave velocity model. Depth is indicated in the upper left corner. Note the different velocity scale for each figure. White colour always shows the mean shear velocity of the depth section. Results are only shown for the areas with good resolution.

s at ~22 km.

4.4. Vienna basin

The second major low velocity zone, and maybe the most interesting region in the study area is the NE Vienna basin and its surroundings at the triple junction of the Austrian, Slovak and Czech border. Although topographically the Little Carpathians separate the Vienna basin from the Danube basin, yet they appear as one low shear velocity region in the uppermost crust characterized by around 2.6–3.0 km/s shear velocities in the uppermost ~6 km, with only slightly higher velocities beneath the Little Carpathians (Fig. 10). The low velocities can be tracked down to 6–9 km in the Danube basin, and even deeper beneath the Vienna basin, where the 2.8 km/s isovelocity contour line reaches approx. 12 km depth (Fig. 11). The low shear velocity anomaly appears in every noise tomographic study of the area (e.g. Yang et al., 2007; Ren et al., 2013; Behm et al., 2016; Schippkus et al., 2018).

The Vienna basin has a thinner sedimentary filling, than the Danube basin (Fig. 2), but appears on the Bouguer anomaly map with lower values, which suggests that the anomaly cannot be explained only by the difference in the thickness of the sedimentary cover. This is in good agreement with our results, according to which the low velocities extend down to 24 km at least, and are still visible at 29 km depth. The Vienna basin hosts several hydrocarbon fields (Tari, 2005), which could be partially a reason for the extreme low velocities detected near the surface.

Several reflection and wide-angle refraction seismic studies have examined the subduction of the European platform beneath the Carpathian arc. The reflection profile, discussed in Tomek and Hall (1993), shows the east-dipping, partially subducted Bohemian Massif beneath the accretional wedge; and in southeast continuation the Vienna basin can be seen as a narrow, pull-apart trough. Hrubcová and Środa (2015) prove, based on CELEBRATION2000 and SUDETES2003 profiles, that a step-like Moho topography from 28 to 38 km depth is present at the contact of the Bohemian Massif and the Carpathians, a few tens of kilometres NW to the Vienna basin. It's worth mentioning, that the CEL09 profile shows an approx. 8 km deep basin at the Carpathian foredeep, but does not show low P wave velocities in middle crustal depths beneath the Vienna basin (Hrubcová and Środa, 2015). This line segment runs parallel to the north-western end of AA' cross-section in Fig. 11, which shows a low velocity anomaly very similar in shape, fast deepening towards the Vienna basin. Our cross-section shows the continuation and further deepening of this basin, however, in the seismic profiles it is confined to the territory beneath the Outer Carpathians.

The Vienna basin is also associated with higher electric conductivity (Jankowski et al., 1985, 2008), positive magnetic anomaly (Blaumoser, 1991), lower surface heat flow [Lenkey et al., 2002] and high gradient in the integrated lithospheric strength (Bada et al., 2007).

The origin of this low S velocity anomaly beneath the Vienna basin is still the subject of debate. Theoretically, low crustal shear velocities can be caused by low density materials, zones of ductile deformation, high temperature or the presence of fluids.

Beneath the Vienna basin Novotný (2012) mapped a low P velocity

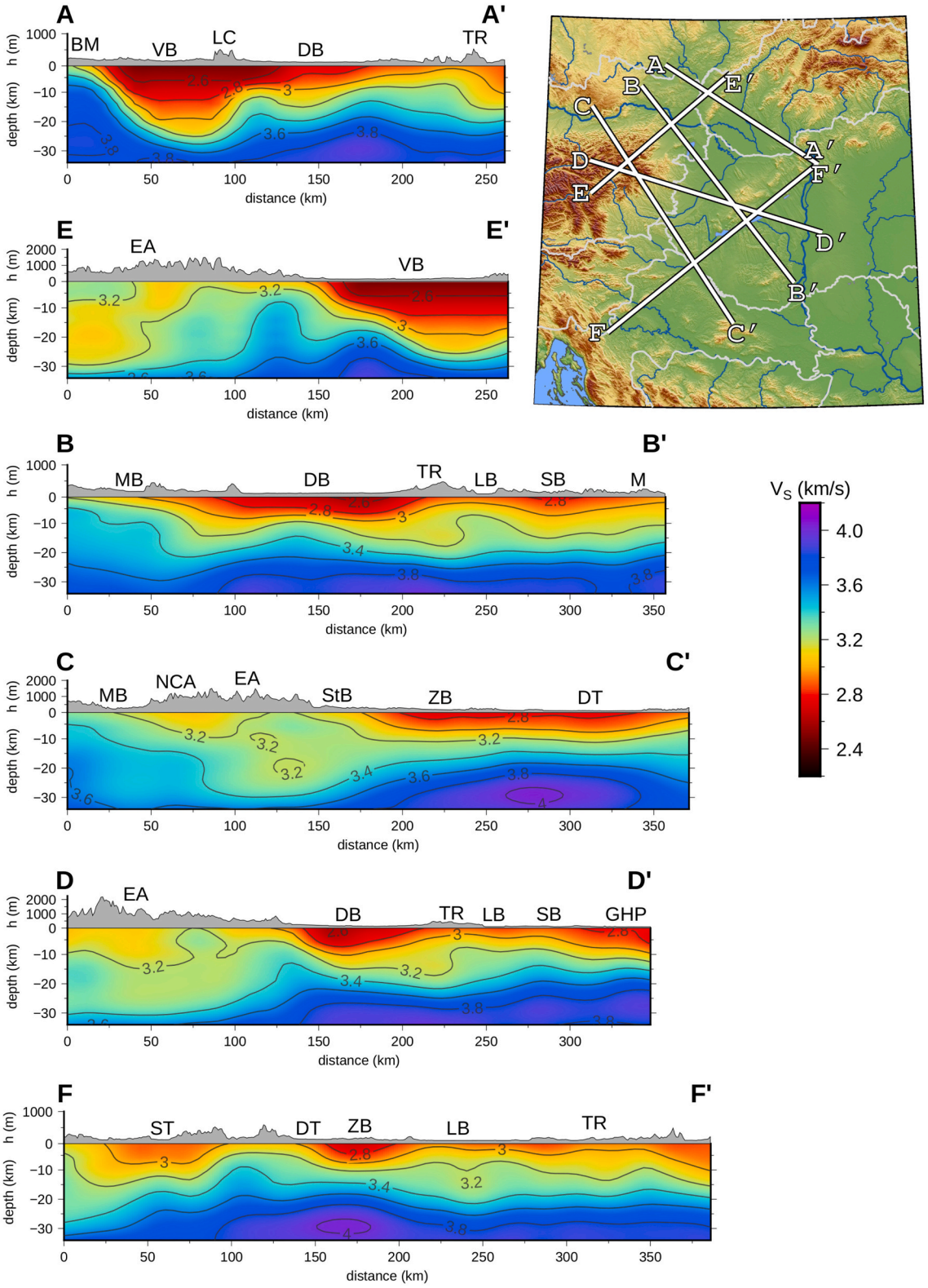

Fig. 11. Cross-sections of the S wave velocity structure along selected profiles. Abbreviations: BM – Bohemian Massif, DB – Danube basin, DT – Drava trough, EA – Eastern Alps, GHP – Great Hungarian Plain, LC – Little Carpathians, LB – Lake Balaton, M – Mecsek, MB – Molasse basin, NCA – Northern Calcareous Alps, SB – Somogy basin, ST – Sava trough, StB – Styrian basin, TR – Transdanubian Range, VB – Vienna basin, ZB – Zala basin. Profile BB' runs along the CEL08 line, and CC' profile along CEL07 line of the CELEBRATION 2000 project.

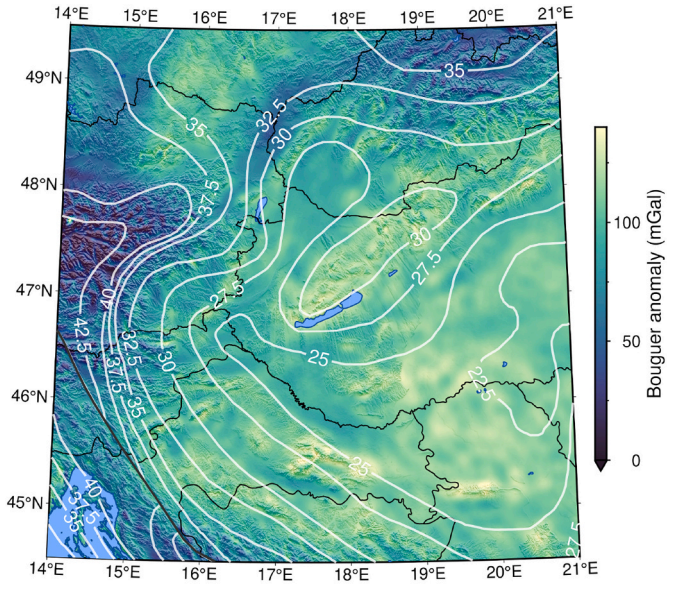

Fig. 12. Bouguer anomaly map of the study region extracted from the World Gravity Map 2012 (Bonvalot et al., 2012) shows generally positive values for the region, negative anomalies can be observed only at the Eastern Alps. Moho depth after Horváth et al. (2015) is indicated by white lines.

anomaly, and interpreted it as pre-Tertiary deposits dragged downwards with the progressing of the Carpathian nappes and suggested that the mass transfer associated with basin subsidence was continuing beyond 20 km depth, which could explain the observed low shear velocities.

The Rayleigh and Love wave phase-velocity maps by Soomro et al. (2016) show significant velocity difference at periods corresponding to mid-crustal depths beneath the territory of NE Vienna basin, suggesting anisotropy, therefore potential ductile deformation in the middle crust. Although the SW Vienna basin exhibit substantial seismicity, the lack of earthquakes at the low shear velocity anomaly (Hausmann et al., 2010) supports this hypothesis.

The surface heat flow in the Vienna basin is relatively low (e.g. Lenkey et al., 2002), therefore a thermal origin of the low shear velocities is not likely.

The Vienna basin is a narrow, deep sedimentary basin, therefore pressure beneath it is lower than in the surrounding crust, causing lateral pressure gradient, similar to what we can see at the Dead Sea basin (ten Brink et al., 2006). This might induce fluid migration towards the basin area and fluids originating from the neighbouring crust or the upper mantle might stall at the brittle-ductile transition in the crust, causing the observed low shear velocities in the middle crust.

4.5. Transdanubian Range

The Transdanubian Range is located at the SE edge of the ALCAPA unit, and lies between the Danube basin and the Mid-Hungarian Zone. The BB' profile (Fig. 11) runs along the CEL08 line of the CELEBRATION2000 project. It crosses the Transdanubian Range and reveals the thicker crust beneath it compared to the Danube basin, similar to the seismic section presented by Kiss (2009).

The crustal structure at the Transdanubian Range, similar to the results of Ren et al. (2013), shows a low vertical shear velocity gradient (Fig. 11, BB' profile), which may be related to less depth-dependent densities. This is supported by the Bouguer anomaly map, where it is imaged with one of the highest positive values, implying significant excess weight compared to the local average crust. The extra mass comes from the lack of sedimentary cover.

Compared to the 24 km depth section, where the Transdanubian Range is still clearly visible, at 29 km depth the shear velocities in the Pannonian basin show a relatively uniform pattern, suggesting that the Moho beneath the Transdanubian Range is approximately at 29 km depth and even shallower beneath the other areas.

The Transdanubian Range is a relatively low mountain range, but it clearly has crustal root embedded in the higher velocity mantle material, as it is obvious from the depth sections in Fig. 10. Based on lower crustal xenoliths and xenocrysts embedded in Plio-Pleistocene alkaline basalts of the Bakony Balaton Highland area an underplated layer composed of basaltic cumulates, metapelitic and mafic granulite xenoliths is present at the Moho beneath the area (Embey-Isztin et al., 1990; Kovács and Szabó, 2005; Török, 2012; Jankovics et al., 2016). These rocks are on average denser than typical lower crustal materials, but less dense than ambient upper mantle (Hacker and Abers, 2004). The presence of this layer up to a few kilometres in thickness was also confirmed by other independent studies as well (Embey-Isztin et al., 1990; Szalay et al., 2011).

Compared to the Moho map of Janik et al. (2011) or Horváth et al. (2015) (Fig. 2b), where the Moho beneath the Transdanubian Range is marked at a depth of 30 km and slightly more, we found the Moho at a somewhat shallower depth. The previous results rely heavily on seismic refraction studies, however the imaging of the underplated material might differ for the two methods, causing the observed differences in the depth of the Moho.

4.6. Drava and Sava troughs

The profile CC' runs in the axis of the Drava trough, on the same path as the CEL07 line of the CELEBRATION2000 project. The interpreted section (Fig. 6. and 8. in Posgay et al., 2007) shows similarity with the results of this study. As for the Drava trough, in both profiles the sedimentary filling is marked by low velocities. This is also true for the Zala basin.

The Alp07 profile of the Alp2002 experiment runs slightly south to our FF' profile. The velocity model of Šumanovac et al. (2016) shows similarities beneath the Drava trough, however, it differs significantly beneath the Sava trough as in our profile, the latter is marked by a 50 km wide, slightly low velocity region of 2.9–3.0 km/s shear velocities in the uppermost crust, which does not occur on the joint interpretation of seismic refraction measurements and receiver function analysis of Šumanovac et al. (2016). However, in both sections the mid-crustal velocity isolines (Vs = 3.2 km/s at approx. 15 km depth in our model) beneath the wider Sava trough area are subhorizontal, and the higher velocity contour lines (e.g. 3.4 km/s) dip from the Sava trough towards the Dinarides.

This region was also included in the study of Ren et al. (2013). The near surface, low velocity anomaly beneath the Sava trough also appears on their depth sections of 2 km and 6 km, with velocities of approx. 2.4 and 2.8 km/s, respectively.

4.7. The Mid-Hungarian Zone

The ambient noise study of Ren et al. (2013) shows a 50–60 km wide, elongated, high velocity zone in their group velocity distribution maps, which they associated with the MHZ, however, in the depth sections this anomaly appears less pronounced, it might be recognized at 10 km, but cannot be seen at greater depths. The MHZ is built up of remnants of oceanic realms (Csontos and Vörös, 2004; Schmid et al., 2008), therefore it should be represented by higher velocities, than the average continental crust. However, despite the achieved relatively high resolution, neither our depth sections, nor our cross-sections show obvious velocity anomaly corresponding to the MHZ.

4.8. Eastern Alps and Western Carpathians

In general, the Eastern Alps show shear velocities with small vertical gradient, only a slight velocity increase can be observed with depth. At

the surface, it is imaged with 3.0–3.1 km/s shear velocities, at 19 km, it is somewhere around 3.2–3.5 km/s, while at 29 km, it is still mapped by 3.2–3.6 km/s velocities (Figs. 10 and 11). The lack of significant velocity increase at 19–29 km depths indicate a deeper Moho beneath the Eastern Alps, than beneath the Pannonian basin. This is in good agreement with the Bouguer anomaly map (Fig. 12), as it shows the Eastern Alps with negative anomaly values, indicating mass deficit.

Nevertheless, the velocities beneath the southern part of the Western Carpathians, where the Central Slovakian Volcanic Area (Szabó et al., 1992, CSVA in Fig. 1) lies, show more vertical variability in the velocities (Fig. 10). At the surface and in the uppermost crust, it is mapped with similar velocities as the Eastern Alps, however, at 19 km it is imaged by higher velocities, similar to the Danube basin and the Drava trough. The high velocities suggest a thinned crust in these territories, possibly including the lack of crustal root, similar to the findings of Szafián and Horváth (2006); Bielik et al. (2018) and Šimonová et al. (2019). The elevated position of the upper mantle beneath the area may also explain the long-lasting Neogene calc-alkaline volcanic activity in this area (Harangi, 2001; Seghedi et al., 2004; Szakács et al., 2018).

5. Conclusions

Based on ambient seismic noise data we determined the crustal shear wave velocity structure for the transition zone between the Eastern Alps and the Pannonian basin through a direct inversion method. The checkerboard tests show that horizontal resolution of 0.2° was achieved for the study region in the upper and middle crust, and 0.3°-0.5° resolution was obtained in the lower crust; thus, our model improves the lateral resolution of former tomographic studies encompassing western Hungary.

The newly defined 3D shear wave velocity structure is in good agreement with near surface geology and gravitational anomalies. The observed structures often correlate well with the seismic reflection and refraction studies, the differences might be due to different resolving capabilities on the one hand, and the types of the used waves on the other hand.

The locations of sediment depocenters, such as the Danube basin, the Vienna basin, the Zala and Somogy basins and the Drava and Sava through could be clearly identified. Beneath the deep sedimentary Danube basin, the upper part of the crust is characterized by very low S wave velocities. Exposed basement in the Bohemian Massif, Eastern Alps, Dinarides, Western Carpathians and the Transdanubian Range explains high near-surface velocities in these regions. Under these mountain ranges the crustal velocities change slightly with depth, suggesting a relatively homogeneous structure, and the thickening of the crust is clearly visible, with the exception of the Central Slovakian Volcanic Area in the Western Carpathians, where relatively high shear velocities were observed at the same depths as beneath the basin areas, indicating the lack of a crustal root.

Although according to Horváth et al. (2006), Janik et al. (2011) and Horváth et al. (2015) the depth of the Moho beneath the Transdanubian Range exceeds 30 km, we interpret it slightly shallower. However, the discrepancy might be partially explained by the underplated material beneath the Bakony Balaton Highland area up to a few kilometres in thickness.

An extremely deep low velocity anomaly was mapped beneath the Vienna basin. The possible mechanisms, which could produce low shear velocities include sediment transfer to the lower crust; ductile deformation suggested by seismic anisotropy; and the presence of fluids.

Although it is possible to identify the MHZ on seismic reflection profiles (e.g. Horváth et al., 2015), we were not capable to distinguish the ALCAPA, Tisza-Dacia micro-terrains and the MHZ by our shear wave velocity model, despite their different composition and origin. As the velocity anomalies appear differently by various imaging techniques, the true properties and existence of the Mid-Hungarian Zone as shear wave velocity anomaly remain ambiguous.

Funding

This work was supported by the Hungarian National Research, Development and Innovation Fund (No. K124241 and 2018-1.2.1-NKP-2018-00007) and the MTA EK Lendület Pannon LithH_2Oscope Research Group.

Declaration of Competing Interest

None.

Acknowledgements

The authors are grateful to all their co-team members within the AlpArray Seismic Network Team: György HETÉNYI, Rafael ABREU, Ivo ALLEGRETTI, Maria-Theresia APOLONER, Coralie AUBERT, Simon BESANÇON, Maxime BÈS DE BERC, Götz BOKELMANN, Didier BRUNEL, Marco CAPELLO, Martina ČARMAN, Adriano CAVALIERE, Jérôme CHÈZE, Claudio CHIARABBA, John CLINTON, Glenn COUGOULAT, Wayne C. CRAWFORD, Luigia CRISTIANO, Tibor CZIFRA, Ezio D'ALEMA, Stefania DANESI, Romuald DANIEL, Anke DANNOWSKI, Iva DASOVIĆ, Anne DESCHAMPS, Jean-Xavier DESSA, Cécile DOUBRE, Sven EGDORF, ETHZ-SED Electronics Lab, Tomislav FIKET, Kasper FISCHER, Wolfgang FRIEDERICH, Florian FUCHS, Sigward FUNKE, Domenico GIARDINI, Aladino GOVONI, Gidera GRÖSCHL, Stefan HEIMERS, Ben HEIT, Davorka HERAK, Marijan HERAK, Johann HUBER, Dejan JARIĆ, Petr JEDLIČKA, Yan JIA, Hélène JUND, Edi KISSLING, Stefan KLINGEN, Bernhard KLOTZ, Petr KOLÍNSKÝ, Heidrun KOPP, Michael KORN, Josef KOTEK, Lothar KÜHNE, Krešo KUK, Dietrich LANGE, Jürgen LOOS, Sara LOVATI, Deny MALENGROS, Lucia MARGHERITI, Christophe MARON, Xavier MARTIN, Marco MASSA, Francesco MAZZARINI, Thomas MEIER, Laurent MÉTRAL, Irene MOLINARI, Milena MORETTI, Anna NARDI, Jurij PAHOR, Anne PAUL, Catherine PÉQUEGNAT, Daniel PETERSEN, Damiano PESARESI, Davide PICCININI, Claudia PIROMALLO, Thomas PLENEFISCH, Jaroslava PLOMEROVÁ, Silvia PONDRELLI, Snježan PREVOLNIK, Roman RACINE, Marc RÉGNIER, Miriam REISS, Joachim RITTER, Georg RÜMPKER, Simone SALIMBENI, Marco SANTULIN, Werner SCHERER, Sven SCHIPPKUS, Detlef SCHULTE-KORTNACK, Vesna ŠIPKA, Stefano SOLARINO, Daniele SPALLAROSSA, Kathrin SPIEKER, Josip STIPČEVIĆ, Angelo STROLLO, Bálint SÜLE, Eszter SZŰCS, Christine THOMAS, Martin THORWART, Frederik TILMANN, Stefan UEDING, Massimiliano VALLOCCHIA, Luděk VECSEY, René VOIGT, Joachim WASSERMANN, Zoltán WÉBER, Christian WEIDLE, Viktor WESZTERGOM, Gauthier WEYLAND, Stefan WIEMER, Felix WOLF, David WOLYNIEC, Thomas ZIEKE, Mladen ŽIVČIĆ and Helena ŽLEBČÍKOVÁ.

We acknowledge the operation of numerous permanent networks in the region, listed at http://www.alparray.ethz.ch/en/seismic_network/backbone/data-policy-and-citation/ and the AlpArray Temporary Seismic Network Z3 (AlpArray Seismic Network, 2015). More information on AlpArray can be found at http://www.alparray.ethz.ch/.

We are indebted to Bruno Goutorbe who made his ambient seismic noise tomographic software package publicly available (http://github.com/bgoutorbe/seismic-noise-tomography). We are grateful to Hongjian Fang, who made his direct inversion program DSurfTomo public (https://github.com/HongjianFang/DSurfTomo). We would like to thank the University of Leeds, SEIS-UK and IRIS DMC for making freely available the data of the Carpathian Basin Project and the South Carpathian Project. The International Gravimetric Bureau is thanked for the Bouguer anomaly map. Maps and plots were generated using the Generic Mapping Tools (Wessel et al., 2013).

We appreciate the anonymous reviewers for their constructive comments which helped to improve the manuscript.

References

Ádám, A., Bielik, M., 1998. The crustal and upper-mantle geophysical signature of narrow continental rifts in the Pannonian basin. Geophys. J. Int. 134, 157–171. https://doi.org/10.1046/j.1365-246x.1998.00544.x.

Ádám, A., Szarka, L., Novák, A., Wesztergom, V., 2017. Key results on deep electrical conductivity anomalies in the Pannonian Basin (PB), and their geodynamic aspects. Acta Geodaetica et Geophysica 52, 205–228. https://doi.org/10.1007/s40328-016-0192-2.

AlpArray Seismic Network, 2015. AlpArray Seismic Network (AASN) Temporary Component. AlpArray Working Group, Other/Seismic Network. https://doi.org/10.12686/alparray/z3_2015.

Artemieva, I.M., Thybo, H., 2013. EUNAseis: A seismic model for Moho and crustal structure in Europe, Greenland, and the North Atlantic region. Tectonophysics 609, 97–153. https://doi.org/10.1016/j.tecto.2013.08.004.

Bada, G., Grenerczy, G., Tóth, L., Horváth, F., Stein, S., Cloetingh, S., Windhoffer, G., Fodor, L., Pinter, N., Fejes, I., 2007. Motion of Adria and ongoing inversion of the Pannonian Basin: Seismicity, GPS velocities, and stress transfer. Special Papers-Geological Society Of America 425, 243.

Baroň, I., Plan, L., Sokol, L., Grasemann, B., Melichar, R., Mitrovic, I., Stemberk, J., 2019. Present-day kinematic behaviour of active faults in the Eastern Alps. Tectonophysics 752, 1–23. https://doi.org/10.1016/j.tecto.2018.12.024.

Bassin, C., Laske, G., Masters, G., 2000. The current limits of resolution for surface wave tomography in North America. EOS 81, F897.

Behm, M., Nakata, N., Bokelmann, G., 2016. Regional Ambient Noise Tomography in the Eastern Alps of Europe. Pure Appl. Geophys. 173, 2813–2840. https://doi.org/10.1007/s00024-016-1314-z.

Bem, T.S., Yao, H., Luo, S., Yang, Y., Wang, X., Wang, X., Li, L., Liu, B., 2020. High-resolution 3-D crustal shear-wave velocity model reveals structural and seismicity segmentation of the central-southern Tanlu Fault zone, eastern China. Tectonophysics 778, 228372. https://doi.org/10.1016/j.tecto.2020.228372.

Bensen, G.D., Ritzwoller, M.H., Barmin, M.P., Levshin, A.L., Lin, F., Moschetti, M.P., Shapiro, N.M., Yang, Y., 2007. Processing seismic ambient noise data to obtain reliable broad-band surface wave dispersion measurements. Geophys. J. Int. 169, 1239–1260. https://doi.org/10.1111/j.1365-246X.2007.03374.x.

Bensen, G., Ritzwoller, M., Yang, Y., 2009. A 3-D shear velocity model of the crust and uppermost mantle beneath the United States from ambient seismic noise. Geophys. J. Int. 177, 1177–1196. https://doi.org/10.1111/j.1365-246X.2009.04125.x.

Bielik, M., Makarenko, I., Csicsay, K., Legostaeva, O., Starostenko, V., Savchenko, A., Šimonová, B., Dérerová, J., Fojtková, L., Pašteka, R., et al., 2018. The refined Moho depth map in the Carpathian-Pannonian region. Contributions to Geophysics and Geodesy 48, 179–190. https://doi.org/10.2478/congeo-2018-0007.

Blaumoser, N., 1991. Eine erste gesamte aeromagnetische Karte von Österreich und ihre Transformationen. Mitt. Österr. Geol. Ges 84, 185–203.

Bonvalot, S., Balmino, G., Briais, A., Kuhn, M., Peyrefitte, A., Vales, N., Biancale, R., Gabalda, G., Reinquin, F., Sarrailh, M., 2012. World gravity map. In: Commission for the Geological Map of the World. Eds. Technical Report. BGI-CGMW-CNES-IRD, Paris.

Bus, Z., 2004. A Kárpát-medence szeizmikus hullámsebesség-eloszlásának tomográfiai vizsgálata. Ph.D. thesis. Eötvös Loránd Tudományegyetem.

ten Brink, U.S., Al-Zoubi, A.S., Flores, C.H., Rotstein, Y., Qabbani, I., Harder, S.H., Keller, G.R., 2006. Seismic imaging of deep low-velocity zone beneath the Dead Sea basin and transform fault: Implications for strain localization and crustal rigidity. Geophys. Res. Lett. 33 https://doi.org/10.1029/2006GL027890.

Brocher, T.M., 2005. Empirical relations between elastic wavespeeds and density in the Earth's crust. Bull. Seismol. Soc. Am. 95, 2081–2092. https://doi.org/10.1785/0120050077.

Brückl, E., Bodoky, T., Hegedűs, E., Hrubcová, P., Gosar, A., Grad, M., Guterch, A., Hajnal, Z., Keller, G.R., Špičák, A., Šumanovac, F., Thybo, H., Weber, F., Alp 2002 Working Group, 2003. Special contribution: ALP 2002 seismic experiment. Stud. Geophys. Geod. 47, 671–679.

Christensen, N.I., Mooney, W.D., 1995. Seismic velocity structure and composition of the continental crust: A global view. Journal of Geophysical Research: Solid Earth 100, 9761–9788. https://doi.org/10.1029/95JB00259.

Csontos, L., Vörös, A., 2004. Mesozoic plate tectonic reconstruction of the Carpathian region. Palaeogeogr. Palaeoclimatol. Palaeoecol. 210, 1–56. https://doi.org/10.1016/j.palaeo.2004.02.033.

Csontos, L., Márton, E., Wórum, G., Benkovics, L., 2002. Geodynamics of SW-Pannonian inselbergs (Mecsek and Villány Mts, SW Hungary): Inferences from a complex structural analysis. EGU Müller Special Pub. Ser 3, 1–19.

Dando, B.D.E., Stuart, G.W., Houseman, G.A., Hegedűs, E., Brückl, E., Radovanović, S., 2011. Teleseismic tomography of the mantle in the Carpathian–Pannonian region of central Europe. Geophys. J. Int. 186, 11–31. https://doi.org/10.1111/j.1365-246X.2011.04998.x.

Decker, K., Peresson, H., Hinsch, R., 2005. Active tectonics and Quaternary basin formation along the Vienna Basin Transform fault. Quat. Sci. Rev. 24, 305–320. https://doi.org/10.1016/j.quascirev.2004.04.012.

Embey-Isztin, A., Scharbert, H., Dietrich, H., Poultidis, H., 1990. Mafic granulites and clinopyroxenite xenoliths from the Transdanubian Volcanic Region (Hungary): implications for the deep structure of the Pannonian Basin. Mineral. Mag. 54, 463–483. https://doi.org/10.1180/minmag.1990.054.376.12.

Fang, H., Zhang, H., 2014. Wavelet-based double-difference seismic tomography with sparsity regularization. Geophys. J. Int. 199, 944–955. https://doi.org/10.1093/gji/ggu305.

Fang, H., Yao, H., Zhang, H., Huang, Y.C., van der Hilst, R.D., 2015. Direct inversion of surface wave dispersion for three-dimensional shallow crustal structure based on ray tracing: methodology and application. Geophys. J. Int. 201, 1251–1263. https://doi.org/10.1093/gji/ggv080.

Fodor, L., 1995. From transpression to transtension: Oligocene-Miocene structural evolution of the Vienna basin and the East Alpine-Western Carpathian junction. Tectonophysics 242, 151–182. https://doi.org/10.1016/0040-1951(94)00158-6.

Fodor, L., Csontos, L., Bada, G., Györfi, I., Benkovics, L., 1999. Tertiary tectonic evolution of the Pannonian Basin system and neighbouring orogens: a new synthesis of palaeostress data. Geol. Soc. Lond., Spec. Publ. 156, 295–334.

van Gelder, I., Willingshofer, E., Sokoutis, D., Cloetingh, S., 2017. The interplay between subduction and lateral extrusion: A case study for the European Eastern Alps based on analogue models. Earth Planet. Sci. Lett. 472, 82–94. https://doi.org/10.1016/j.epsl.2017.05.012.

González-Vidal, D., Obermann, A., Tassara, A., Bataille, K., Lupi, M., 2018. Crustal model of the Southern Central Andes derived from ambient seismic noise Rayleigh-wave tomography. Tectonophysics 744, 215–226. https://doi.org/10.1016/j.tecto.2018.07.004.

Goutorbe, B., Coelho, D.L.D.O., Drouet, S., 2015. Rayleigh wave group velocities at periods of 6–23 s across Brazil from ambient noise tomography. Geophys. J. Int. 203, 869–882. https://doi.org/10.1093/gji/ggv343.

Grászer, Z., Szanyi, G., Bondár, I., Czanik, C., Czifra, T., Győri, E., Hetényi, G., Kovács, I., Molinari, I., Süle, B., Szűcs, E., Wesztergom, V., Wéber, Z., AlpArray Working Group, 2018. AlpArray in Hungary: temporary and permanent seismological networks in the transition zone between the Eastern Alps and the Pannonian basin. Acta Geodaetica et Geophysica 221–245. https://doi.org/10.1007/s40328-018-0213-4.

Guterch, A., Grad, M., Špičák, A., Brückl, E., Hegedűs, E., Keller, G.R., Thybo, H., CELEBRATION 2000, ALP 2002, SUDETES 2003 Working Groups, 2003. Special contribution: an overview of recent seismic refraction experiments in Central Europe. Stud. Geophys. Geod. 47, 651–657. https://doi.org/10.1023/A:1024775921231.

Guterch, A., Grad, M., Keller, G., 2007. Crust and lithospheric structure–long range controlled source seismic experiments in Europe. Treatise on Geophysics 1, 533–558. https://doi.org/10.1016/B978-044452748-6.00016-X.

Haas, J., Budai, T., Csontos, L., Fodor, L., Konrád, G., Koroknai, B., 2014. Geology of the Pre-Cenozoic Basement of Hungary: Explanatory Notes for Pre-Cenozoic Geological Map of Hungary, 1: 500 000. Geological and Geophysical Institute of Hungary.

Hacker, B.R., Abers, G.A., 2004. Subduction Factory 3: An Excel worksheet and macro for calculating the densities, seismic wave speeds, and H_2O contents of minerals and rocks at pressure and temperature. Geochem. Geophys. Geosyst. 5 https://doi.org/10.1029/2003GC000614.

Harangi, S., 2001. Neogene to Quaternary volcanism of the Carpathian–Pannonian Region—a review. Acta Geol. Hung. 44, 223–258.

Harangi, S., Downes, H., Thirlwall, M., Gméling, K., 2007. Geochemistry, petrogenesis and geodynamic relationships of Miocene calc-alkaline volcanic rocks in the Western Carpathian arc, Eastern Central Europe. J. Petrol. 48, 2261–2287. https://doi.org/10.1093/petrology/egm059.

Hausmann, H., Hoyer, S., Schurr, B., Brueckl, E., Houseman, G., Stuart, G., 2010. New seismic data improve earthquake location in the Vienna basin area, Austria. Austrian Journal of Earth Sciences 103, 2–14.

Herrmann, R.B., Ammon, C.J., 2002. Computer Programs in Seismology: Surface Waves, Receiver Functions and Crustal Structure. Saint Louis University, Missouri.

Hetényi, G., Bus, Z., 2007. Shear wave velocity and crustal thickness in the Pannonian Basin from receiver function inversions at four permanent stations in Hungary. J. Seismol. 11, 405–414. https://doi.org/10.1007/s10950-007-9060-4.

Hetényi, G., Stuart, G.W., Houseman, G.A., Horváth, F., Hegedűs, E., Brückl, E., 2009. Anomalously deep mantle transition zone below Central Europe: Evidence of lithospheric instability. Geophys. Res. Lett. 36, L21307 https://doi.org/10.1029/2009GL040171.

Hetényi, G., Ren, Y., Dando, B., Stuart, G.W., Hegedűs, E., Kovács, A.C., Houseman, G.A., 2015. Crustal structure of the Pannonian Basin: The AlCaPa and Tisza Terrains and the Mid-Hungarian Zone. Tectonophysics 646, 106–116. https://doi.org/10.1016/j.tecto.2015.02.004.

Hetényi, G., Molinari, I., Clinton, J., Bokelmann, G., Bondár, I., Crawford, W.C., Dessa, J. X., Doubre, C., Friederich, W., Fuchs, F., Giardini, D., Grászer, Z., Handy, M.R., Herak, M., Jia, Y., Kissling, E., Kopp, H., Korn, M., Margheriti, L., Meier, T., Mucciarelli, M., Paul, A., Pesaresi, D., Piromallo, C., Plenefisch, T., Plomerová, J., Ritter, J., Rümpker, G., Šipka, V., Spallarossa, D., Thomas, C., Tilmann, F., Wassermann, J., Weber, M., Wéber, Z., Wesztergom, V., Živčić, M., AlpArray Seismic Network Team, AlpArray OBS Cruise Crew, AlpArray Working Group, 2018. The AlpArray Seismic Network: a large-scale European experiment to image the Alpine Orogen. Surv. Geophys. 39, 1009–1033. https://doi.org/10.1007/s10712-018-9472-4.

Hinsch, R., Decker, K., 2011. Seismic slip rates, potential subsurface rupture areas and seismic potential of the Vienna Basin Transfer Fault. Int. J. Earth Sci. 100, 1925–1935. https://doi.org/10.1007/s00531-010-0613-3.

Hölzel, M., Decker, K., Zámolyi, A., Strauss, P., Wagreich, M., 2010. Lower Miocene structural evolution of the central Vienna Basin (Austria). Mar. Pet. Geol. 27, 666–681. https://doi.org/10.1016/j.marpetgeo.2009.10.005.

Horváth, F., 1993. Towards a mechanical model for the formation of the Pannonian basin. Tectonophysics 226, 333–357. https://doi.org/10.1016/0040-1951(93)90126-5.

Horváth, F., 1995. Phases of compression during the evolution of the Pannonian Basin and its bearing on hydrocarbon exploration. Mar. Pet. Geol. 12, 837–844. https://doi.org/10.1016/0264-8172(95)98851-U.

Horváth, F., Bada, G., Szafián, P., Tari, G., Ádám, A., Cloetingh, S.A.P.L., 2006. Formation and deformation of the Pannonian Basin: constraints from observational

data. Geological Society, London, Memoirs 32, 191–206. https://doi.org/10.1144/GSL.MEM.2006.032.01.11.
Horváth, F., Musitz, B., Balázs, A., Végh, A., Uhrin, A., Nádor, A., Koroknai, B., Pap, N., Tóth, T., Wórum, G., 2015. Evolution of the Pannonian basin and its geothermal resources. Geothermics 53, 328–352. https://doi.org/10.1016/j.geothermics.2014.07.009.
Hrubcová, P., Środa, P., 2015. Complex local Moho topography in the Western Carpathians: Indication of the ALCAPA and the European Plate contact. Tectonophysics 638, 63–81. https://doi.org/10.1016/j.tecto.2014.10.013.
Hrubcová, P., Środa, P., Grad, M., Geissler, W., Guterch, A., Vozár, J., Hegedűs, E., 2010. From the Variscan to the Alpine Orogeny: crustal structure of the Bohemian Massif and the Western Carpathians in the light of the SUDETES 2003 seismic data. Geophys. J. Int. 183, 611–633. https://doi.org/10.1111/j.1365-246X.2010.0.
Hu, S., Yao, H., 2018. Crustal velocity structure around the eastern Himalayan syntaxis: Implications for the nucleation mechanism of the 2017 Ms 6.9 Mainling earthquake and regional tectonics. Tectonophysics 744, 1–9. https://doi.org/10.1016/j.tecto.2018.06.006.
Janik, T., Grad, M., Guterch, A., Vozár, J., Bielik, M., Vozárova, A., Hegedűs, E., Kovács, C.A., Kovács, I., Keller, G.R., 2011. Crustal structure of the Western Carpathians and Pannonian Basin: Seismic models from CELEBRATION 2000 data and geological implications. J. Geodyn. 52, 97–113. https://doi.org/10.1016/j.jog.2010.12.002.
Jankovics, M.É., Taracsák, Z., Dobosi, G., Embey-Isztin, A., Batki, A., Harangi, S., Hauzenberger, C.A., 2016. Clinopyroxene with diverse origins in alkaline basalts from the western Pannonian Basin: Implications from trace element characteristics. Lithos 262, 120–134.
Jankowski, J., Tarłowski, Z., Praus, O., Pěčová, J., Petr, V., 1985. The results of deep geomagnetic soundings in the West Carpathians. Geophys. J. Int. 80, 561–574. https://doi.org/10.1111/j.1365-246X.1985.tb05111.x.
Jankowski, J., Jóźwiak, W., Vozár, J., 2008. Arguments for ionic nature of the Carpathian electric conductivity anomaly. Acta Geophysica 56, 455–465. https://doi.org/10.2478/s11600-008-0004-3.
Kalmár, D., Hetényi, G., Bondár, I., 2019. Moho depth analysis of the eastern Pannonian Basin and the Southern Carpathians from receiver functions. J. Seismol. 23, 967–982. https://doi.org/10.1007/s10950-019-09847-w.
Kilényi, E., Šefara, J., 1989. Pre-Tertiary Basement Contour Map of the Carpathian Basin beneath Austria, Czechoslovakia and Hungary. Eötvös Loránd Geophys. Inst.
Kiss, J., 2009. A CEL08 szelvény geofizikai vizsgálata (Study of the geophysical data along the CEL08 deep seismic litospheric profile). Magyar Geofizika 50, 59–74.
Kiss, J., 2016. A gravitációs és mágneses anomáliák átfogó értelmezése a Kárpát–Pannon-régióban/Comprehensive interpretation of gravity and magnetic anomalies in Carpathian–Pannonian Region. Földtani Közlöny 146, 275–298.
Kováč, M., Márton, E., Klučiar, T., Vojtko, R., 2018. Miocene basin opening in relation to the north-eastward tectonic extrusion of the ALCAPA Mega-Unit. Geol. Carpath. 69, 254–263. https://doi.org/10.1515/geoca-2018-0015.
Kovács, I., Szabó, C., 2005. Petrology and geochemistry of granulite xenoliths beneath the Nógrád-Gömör volcanic field, Carpathian-Pannonian region (N-Hungary/S-Slovakia). Mineral. Petrol. 85, 269–290. https://doi.org/10.1007/s00710-005-0090-8.
Kovács, I., Szabó, C., 2008. Middle Miocene volcanism in the vicinity of the Middle Hungarian zone: evidence for an inherited enriched mantle source. J. Geodyn. 45, 1–17. https://doi.org/10.1016/j.jog.2007.06.002.
Kovács, I., Falus, G., Stuart, G., Hidas, K., Szabó, C., Flower, M., Hegedűs, E., Posgay, K., Zilahi-Sebess, L., 2012. Seismic anisotropy and deformation patterns in upper mantle xenoliths from the central Carpathian–Pannonian region: Asthenospheric flow as a driving force for Cenozoic extension and extrusion? Tectonophysics 514, 168–179. https://doi.org/10.1016/j.tecto.2011.10.022.
Kovács, I., Patkó, L., Liptai, N., Lange, T., Taracsák, Z., Cloetingh, S., Török, K., Király, E., Karátson, D., Biró, T., Kiss, J., Pálos, Z., Aradi, L., Falus, G., Hidas, K., Berkesi, M., Koptev, A., Novák, A., Wesztergom, V., Fancsik, T., Szabó, C., 2020. The role of water and compression in the genesis of alkaline basalts: Inferences from the Carpathian-Pannonian region. Lithos 354–355, 105323. https://doi.org/10.1016/j.lithos.2019.105323.
Lankreijer, A.C., Kovac, M., Cloetingh, S., Pitonak, P., Hloska, M., Biermann, C., 1995. Quantitative subsidence analyses and forward modelling in the Vienna and Danube basins. Tectonophysics 252, 470–484.
Laske, G., Masters, G., Ma, Z., Pasyanos, M., 2013. Update on CRUST1.0 — A 1-degree global model of Earth's crust. In: Geophys. Res. Abstr, EGU General Assembly Vienna, Austria, p. 2658.
Lee, E.Y., Wagreich, M., 2017. Polyphase tectonic subsidence evolution of the Vienna Basin inferred from quantitative subsidence analysis of the northern and central parts. Int. J. Earth Sci. 106, 687–705. https://doi.org/10.1007/s00531-016-1329-9.
Legendre, C.P., Tseng, T.L., Chen, Y.N., Huang, T.Y., Gung, Y.C., Karakhanyan, A., Huang, B.S., 2017. Complex deformation in the Caucasus region revealed by ambient noise seismic tomography. Tectonophysics 712, 208–220. https://doi.org/10.1016/j.tecto.2017.05.024.
Lenkey, L., Dövényi, P., Horváth, F., Cloetingh, S., 2002. Geothermics of the Pannonian basin and its bearing on the neotectonics. In: Cloetingh, S., Horváth, F., Bada, G., Lankreijer, A. (Eds.), Neotectonics and surface processes: the Pannonian basin and Alpine/Carpathian system, EGU Stephan Mueller Special Publication Series, pp. 29–40.
Lenkey, L., Raáb, D., Goetzl, G., Lapanje, A., Nádor, A., Rajver, D., Rotár-Szalkai, Á., Svasta, J., Zekiri, F., 2017. Lithospheric scale 3D thermal model of the Alpine–Pannonian transition zone. Acta Geodaetica et Geophysica 52, 161–182. https://doi.org/10.1007/s40328-017-0194-8.
Levshin, A., Ritzwoller, M., 2001. Automated detection, extraction, and measurement of regional surface waves. In: Monitoring the Comprehensive Nuclear-Test-Ban Treaty: Surface Waves. Springer, pp. 1531–1545. https://doi.org/10.1007/978-3-0348-8264-4_11.
Liu, M., Shen, Y., 1998. Sierra Nevada uplift: a ductile link to mantle upwelling under the Basin and Range province. Geology 26, 299–302.
Lučić, D., Saftić, B., Krizmanić, K., Prelogović, E., Britvić, V., Mesić, I., Tadej, J., 2001. The Neogene evolution and hydrocarbon potential of the Pannonian Basin in Croatia. Mar. Pet. Geol. 18, 133–147. https://doi.org/10.1016/S0264-8172(00)00038-6.
Luo, S., Yao, H., Li, Q., Wang, W., Wan, K., Meng, Y., Liu, B., 2019. High-resolution 3D crustal S-wave velocity structure of the Middle-Lower Yangtze River Metallogenic Belt and implications for its deep geodynamic setting. Science China Earth Sciences 62, 1361–1378. https://doi.org/10.1007/s11430-018-9352-9.
Márton, E., Fodor, L., 2003. Tertiary paleomagnetic results and structural analysis from the Transdanubian Range (Hungary): rotational disintegration of the Alcapa unit. Tectonophysics 363, 201–224. https://doi.org/10.1016/S0040-1951(02)00672-8.
Márton, E., Kuhlemann, J., Frisch, W., Dunkl, I., 2000. Miocene rotations in the Eastern Alps – palaeomagnetic results from intramontane basin sediments. Tectonophysics 323, 163–182. https://doi.org/10.1016/S0040-1951(00)00102-5.
Molinari, I., Morelli, A., 2011. EPcrust: a reference crustal model for the European Plate. Geophys. J. Int. 185, 352–364. https://doi.org/10.1111/j.1365-246X.2011.04940.x.
Molinari, I., Verbeke, J., Boschi, L., Kissling, E., Morelli, A., 2015. Italian and Alpine three-dimensional crustal structure imaged by ambient-noise surface-wave dispersion. Geochem. Geophys. Geosyst. 16, 4405–4421. https://doi.org/10.1002/2015GC006176.
Mooney, W.D., Laske, G., Masters, T.G., 1998. CRUST 5.1: A global crustal model at 5° × 5°. Journal of Geophysical Research: Solid Earth 103, 727–747. https://doi.org/10.1029/97JB02122.
Nemcok, M., Marko, F., Kovác, M., Fodor, L., 1989. Neogene tectonics and paleostress changes in the Czechoslovakian part of the Vienna Basin. Jahrb. Geol. Bundesanst. 132, 443–458.
Novotný, M., 2012. Depth-recursive tomography of the Bohemian Massif at the CEL09 Transect—Part B: Interpretation. Surv. Geophys. 33, 243–273.
Pécskay, Z., Lexa, J., Szakács, A., Seghedi, I., Balogh, K., Konečný, V., Zelenka, T., Kovacs, M., Póka, T., Fülöp, A., Márton, E., Panaiotu, C., Cvetković, V., 2006. Geochronology of Neogene magmatism in the Carpathian arc and intra-Carpathian area. Geol. Carpath. 57, 511.
Posgay, K., Csabafi, R., Bodoky, T., Hegedűs, E., Fancsik, T., Rigler, B., 2007. A CEL07 mélyszeizmikus szelvény újraértékelése. Magyar Geofizika 48, 87–99.
Ranalli, G., 1995. Rheology of the Earth. Springer Science & Business Media.
Ratschbacher, L., Merle, O., Davy, P., Cobbold, P., 1991. Lateral extrusion in the Eastern Alps, part 1: boundary conditions and experiments scaled for gravity. Tectonics 10, 245–256. https://doi.org/10.1029/90TC02622.
Rawlinson, N., Sambridge, M., 2004. Wave front evolution in strongly heterogeneous layered media using the fast marching method. Geophys. J. Int. 156, 631–647. https://doi.org/10.1111/j.1365-246X.2004.02153.x.
Ren, Y., Grecu, B., Stuart, G.W., Houseman, G.A., Hegedűs, E., SCP Working Group, 2013. Crustal structure of the Carpathian–Pannonian region from ambient noise tomography. Geophys. J. Int. 195, 1351–1369. https://doi.org/10.1093/gji/ggt316.
Ren, Y., Stuart, G.W., Houseman, G.A., Dando, B., Ionescu, C., Hegedűs, E., Radovanović, S., Shen, Y., 2012. Upper mantle structures beneath the Carpathian–Pannonian region: Implications for the geodynamics of continental collision. Earth Planet. Sci. Lett. 349, 139–152. https://doi.org/10.1016/j.epsl.2012.06.037.
Ritzwoller, M.H., Lin, F.C., Shen, W., 2011. Ambient noise tomography with a large seismic array. Compt. Rendus Geosci. 343, 558–570. https://doi.org/10.1016/j.crte.2011.03.007.
Royden, L.H., 1985. The Vienna Basin: A thin-skinned pull-apart basin. In: Biddle, K.T., Christie-Blick, N. (Eds.), Strike-Slip Deformation, Basin Formation, and Sedimentation, SEPM Society for Sedimentary Geology, vol. 37, pp. 319–338. https://doi.org/10.2110/pec.85.37.0303.
Šamajová, L., Hók, J., Bielik, M., Pelech, O., 2018. Deep contact of the Bohemian Massif and Western Carpathians as seen from density modeling. Geol. Carpath. 69, 545–557. https://doi.org/10.1515/geoca-2018-0032.
Šamajová, L., Hók, J., Csibri, T., Bielik, M., Teťák, F., Brixová, B., Sliva, L., Šály, B., 2019. Geophysical and geological interpretation of the Vienna Basin pre-Neogene basement (Slovak part of the Vienna Basin). Geol. Carpath. 70, 418–431. https://doi.org/10.2478/geoca-2019-0024.
Schippkus, S., Zigone, D., Bokelmann, G., AlpArray Working Group, 2018. Ambient-noise tomography of the wider Vienna Basin region. Geophys. J. Int. 215, 102–117. https://doi.org/10.1093/gji/ggy259.
Schmid, S.M., Bernoulli, D., Fügenschuh, B., Matenco, L., Schefer, S., Schuster, R., Tischler, M., Ustaszewski, K., 2008. The Alpine-Carpathian-Dinaridic orogenic system: correlation and evolution of tectonic units. Swiss J. Geosci. 101, 139–183. https://doi.org/10.1007/s00015-008-1247-3.
Sebe, K., Kovačić, M., Magyar, I., Krizmanić, K., Špelić, M., Bigunac, D., Sütő-Szentai, M., Kovács, Á., Szuromi-Korecz, A., Bakrač, K., Hajek-Tadesse, V., Troskot-Čorbić, T., Sztanó, O., 2020. Correlation of upper Miocene–Pliocene Lake Pannon deposits across the Drava Basin, Croatia and Hungary. Geologia Croatica 73, 177–195.
Seghedi, I., Downes, H., Szakács, A., Mason, P.R., Thirlwall, M.F., Roşu, E., Pécskay, Z., Márton, E., Panaiotu, C., 2004. Neogene–Quaternary magmatism and geodynamics in the Carpathian–Pannonian region: a synthesis. Lithos 72, 117–146.
Shapiro, N.M., Campillo, M., 2004. Emergence of broadband Rayleigh waves from correlations of the ambient seismic noise. Geophys. Res. Lett. 31, 5. https://doi.org/10.1029/2004GL019491.

Šimonová, B., Zeyen, H., Bielik, M., 2019. Continental lithospheric structure from the East European Craton to the Pannonian Basin based on integrated geophysical modelling. Tectonophysics 750, 289–300. https://doi.org/10.1016/j.tecto.2018.12.003.

Singer, J., Obermann, A., Kissling, E., Fang, H., Hetényi, G., Grujic, D., 2017. Along-strike variations in the Himalayan orogenic wedge structure in Bhutan from ambient seismic noise tomography. Geochem. Geophys. Geosyst. 18, 1483–1498. https://doi.org/10.1002/2016GC006742.

Soomro, R., Weidle, C., Cristiano, L., Lebedev, S., Meier, T., PASSEQ Working Group, 2016. Phase velocities of Rayleigh and Love waves in central and northern Europe from automated, broad-band, interstation measurements. Geophys. J. Int. 204, 517–534.

Šumanovac, F., Hegedűs, E., Orešković, J., Kolar, S., Kovács, A.C., Dudjak, D., Kovács, I. J., 2016. Passive seismic experiment and receiver functions analysis to determine crustal structure at the contact of the northern Dinarides and southwestern Pannonian Basin. Geophys. J. Int. 205, 1420–1436. https://doi.org/10.1093/gji/ggw101.

Szabó, C., Harangi, S., Csontos, L., 1992. Review of Neogene and Quaternary volcanism of the Carpathian-Pannonian region. Tectonophysics 208, 243–256. https://doi.org/10.1016/0040-1951(92)90347-9.

Szafián, P., Horváth, F., 2006. Crustal structure in the Carpatho-Pannonian region: insights from three-dimensional gravity modelling and their geodynamic significance. Int. J. Earth Sci. 95, 50–67. https://doi.org/10.1007/s00531-005-0488-x.

Szakács, A., Pécskay, Z., Gál, Á., 2018. Patterns and trends of time–space evolution of Neogene volcanism in the Carpathian–Pannonian region: a review. Acta Geodaetica et Geophysica 53, 347–367. https://doi.org/10.1007/s40328-018-0230-3.

Szalay, I., Gúthy, T., Gömböcz, L., 2011. Az 1965–67. évi dunántúli kéregkutató mérések refrakciós tomográfiás feldolgozása. Magyar Geofizika 52, 193–209.

Szanyi, G., Gráczer, Z., Győri, E., 2013. Ambient seismic noise Rayleigh wave tomography for the Pannonian basin. Acta Geodaetica et Geophysica 48, 209–220. https://doi.org/10.1007/s40328-013-0019-3.

Szanyi, G., 2016. Investigations on the S wave Velocity Structure of the Pannonian Basin. Ph.D. thesis. Eötvös Loránd Tudományegyetem, Budapest. https://doi.org/10.15476/ELTE.2016.118 (in Hungarian).

Sztanó, O., Kováč, M., Magyar, I., Šujan, M., Fodor, L., Uhrin, A., Rybár, S., Csillag, G., Tőkés, L., 2016. Late Miocene sedimentary record of the Danube/Kisalföld Basin: interregional correlation of depositional systems, stratigraphy and structural evolution. Geol. Carpath. 67, 525–542.

Tari, G., 1996. Extreme crustal extension in the Rába River extensional corridor (Austria/Hungary). Mitteilungen der Gesellschaft der Geologie-und Bergbaustudenten in Österreich 41, 1–17.

Tari, G., 2005. The divergent continental margins of the Jurassic proto-Pannonian Basin: implications for the petroleum systems of the Vienna Basin and the Moesian Platform. In: 5th Annual Bob. F. Perkins Research Conference: Petroleum Systems of Divergent Continental Margin Basins, pp. 955–986.

Tari, G.C., Horváth, F., 2006. Alpine evolution and hydrocarbon geology of the Pannonian Basin: An overview. In: Golonka, J., Picha, F. (Eds.), The Carphathians and their foreland: Geology and hydrocarbon resources: AAPG Memoir, AAPG Special Volumes., vol. 84. AAPG, pp. 605–618.

Tari, G., Horváth, F., 2010. Eo-Alpine evolution of the Transdanubian range in the nappe system of the Eastern Alps: revival of a 15 years old tectonic model. Földtani Közlöny 140, 483–510.

Tian, X., Teng, J., Zhang, H., Zhang, Z., Zhang, Y., Yang, H., Zhang, K., 2011. Structure of crust and upper mantle beneath the Ordos Block and the Yinshan Mountains revealed by receiver function analysis. Phys. Earth Planet. Inter. 184, 186–193. https://doi.org/10.1016/j.pepi.2010.11.007.

Timkó, M., Kovács, I., Wéber, Z., 2019. 3D P-wave velocity image beneath the Pannonian Basin using traveltime tomography. Acta Geodaetica et Geophysica 54, 373–386. https://doi.org/10.1007/s40328-019-00267-3.

Tomek, C., Hall, J., 1993. Subducted continental margin imaged in the Carpathians of Czechoslovakia. Geology 21, 535–538. https://doi.org/10.1130/0091-7613(1993)021<0535:SCMIIN>2.3.CO;2.

Tondi, R., Vuan, A., Borghi, A., Argnani, A., 2019. Integrated crustal model beneath the Po Plain (Northern Italy) from surface wave tomography and Bouguer gravity data. Tectonophysics 750, 262–279. https://doi.org/10.1016/j.tecto.2018.10.018.

Török, K., 2012. On the origin and fluid content of some rare crustal xenoliths and their bearing on the structure and evolution of the crust beneath the Bakony–Balaton Highland Volcanic Field (W-Hungary). Int. J. Earth Sci. 101, 1581–1597.

Wessel, P., Smith, W.H., Scharroo, R., Luis, J., Wobbe, F., 2013. Generic Mapping Tools: improved version released. EOS Transactions American Geophysical Union 94, 409–410. https://doi.org/10.1002/2013EO450001.

Yang, Y., Ritzwoller, M.H., Levshin, A.L., Shapiro, N.M., 2007. Ambient noise Rayleigh wave tomography across Europe. Geophys. J. Int. 168, 259–274. https://doi.org/10.1111/j.1365-246X.2006.03203.x.

Yudistira, T., Paulssen, H., Trampert, J., 2017. The crustal structure beneath the Netherlands derived from ambient seismic noise. Tectonophysics 721, 361–371. https://doi.org/10.1016/j.tecto.2017.09.025.

Zhang, Y., Yao, H., Yang, H.Y., Cai, H.T., Fang, H., Xu, J., Jin, X., Kuo-Chen, H., Liang, W. T., Chen, K.X., 2018. 3-D crustal shear-wave velocity structure of the Taiwan Strait and Fujian, SE China, revealed by ambient noise tomography. Journal of Geophysical Research: Solid Earth 123, 8016–8031. https://doi.org/10.1029/2018JB015938.